

An integrated framework for river assimilative capacity allocation based on environmental fairness and efficiency trade-offs with a modified optimization model in a river basin

Zhimin Yang^a, Jiangying Wang^b, Xiaoxuan Li^a, Chunhui Li^{a,*}, Zaohong Pu^a, Jing Hu^a, Yujun Yi^{c, **}, Xuan Wang^{a,c}, Qiang Liu^a

^a Key Laboratory for Water and Sediment Sciences of Ministry of Education, School of Environment, Beijing Normal University, Beijing, 100875, China

^b School of Information Science and Engineering, Hunan Normal University, Hunan, 410081, China

^c State Key Laboratory of Water Environment Simulation, School of Environment, Beijing Normal University, Beijing, 100875, China

ARTICLE INFO

Keywords:

River assimilative capacity
Optimization model
Environmental gini coefficient
Fairness and efficiency
MIKE 11 model

ABSTRACT

The allocation of river assimilative capacity (RAC) remains a complex challenge due to the trade-offs between environmental fairness and efficiency. To address these issues, a novel integrated framework for the optimal allocation of RAC was proposed. The Luan River Basin in Chengde City, China, was selected as a case study. Hydrodynamic and advection-dispersion modules from the MIKE 11 model were implemented and then integrated into the RAC model. An orthogonal experimental method was used to identify significant factors influencing RAC, and three regulatory scenarios were designed. The environmental Gini coefficient (EGC) was modified using a probability distribution function to evaluate fairness-based allocation of RAC, and the environmental benefits were used to quantitatively measure efficiency-based allocation. Subsequently, a modified optimization model was developed to determine the optimal RAC allocation under three regulatory scenarios based on environmental fairness and efficiency trade-offs. Results showed that the initial state was the least favorable, with the lowest RAC and highest modified EGC. Under high regulation, the average modified EGC decreased by 68.97 %, 53.49 %, and 18.22 % compared to the initial state, low, and moderate regulation, respectively. High regulation was ideal for environmental fairness. However, when considering the trade-offs between fairness and efficiency, moderate regulation achieved the optimal allocation, minimizing the objective function by 68.64 % compared to high regulation. The study provides new insights into targeted RAC allocation strategies to promote fairness and maintain efficiency.

1. Introduction

Water pollution has become a global concern due to intensive urbanization, rapid industrialization, and agricultural modernization (Xie et al., 2018; Wang et al., 2021, 2025). Excessive use of water resources can impede the self-purification and dilution capabilities of rivers, resulting in water quality deterioration and environmental degradation (Zhao et al., 2018). Additionally, water quality is significantly affected by management practices, allocation, and infrastructure in a changing environment (Zhang et al., 2019). Globally, more than half of the countries and regions face threats from water pollution, which exacerbates the water crisis and inhibits progress toward the United Nations

Sustainable Development Goals (He et al., 2021). Notably, China has suffered from severe water pollution issues, with over 70 % of rivers contaminated (National Bureau of Statistics of China), posing threats to aquatic ecosystems and water security. Therefore, strategic allocation of water pollutant discharges is essential for water quality improvement and sustainable socioeconomic development (Kang et al., 2020).

River assimilative capacity (RAC) is the maximum amount of pollutant discharges that a water body can absorb and assimilate while still meeting specified water quality standards without detrimental effects on the aquatic ecological environment (Lee and Wen, 1996). RAC is also referred to as the total maximum daily load (TMDL) (Haire et al., 2009; Rai et al., 2024), water environmental capacity (Zhao et al., 2018;

* Corresponding author.

** Corresponding author.

E-mail address: chunhuili@bnu.edu.cn (C. Li).

Zhu et al., 2022), and water framework directive (European Commission, 2000). A comprehensive understanding of RAC is imperative for effective pollution control, as it establishes the scientific basis for regulatory measures (Zhang et al., 2019; Yue et al., 2021). Building on this foundation, calculations of RAC quantify the environmental capacity of watersheds, while its allocation determines how pollutant discharge permits are distributed among stakeholders—two key components critical to ecological sustainability and economic development (Liang et al., 2015; Li et al., 2023). For RAC assessment, various calculation methods involve analytical formulas, model trial and error, system optimization, and probabilistic dilution models (USEPA, 1984; Zhu et al., 2022). RAC is influenced by dynamic factors such as river discharges, hydraulic and hydrodynamic conditions, pollution concentrations and sources (Wang et al., 2021; Bui and Pham, 2023). However, most variables are assumed to be constant for RAC calculations (Wang et al., 2019; Feng et al., 2021). To improve the accuracy of RAC assessments, hydrodynamic–water quality models like BOD–DO, S–P, QUAL, WASP, QUASAR, MIKE, BASINS, AQUATOX, and EFDC have been developed (Ji et al., 2022; Zhu et al., 2022). These models simulate river hydrodynamic conditions and pollutant migration and transformation (Chen et al., 2014; Wang et al., 2021). Among these, the MIKE model is widely applied in assessing a river's ability to assimilate pollutants. It incorporates key parameters such as flow rates, water levels, and water quality indices, making it an internationally recognized tool for RAC studies (Chen et al., 2018; Bu et al., 2020). The MIKE 11 model, a process-based hydrodynamic and water quality coupling model, was employed to simulate pollutant transport dynamics and calibrate critical parameters for RAC calculations. Compared with 2D and 3D models, the MIKE 11 model exhibits less reliance on extensive monitoring data and requires simpler boundary conditions, thus demonstrating adaptability for data-scarce rivers when long-term and continuous monitoring is unavailable (DHI, 2005; Zhao et al., 2018; Feng et al., 2021). The model's flexibility allows for parameter adjustments to reflect specific hydrological conditions in targeted water bodies, thereby enabling more accurate RAC results (Bui and Pham, 2023).

How to allocate RAC in a sustainable and stakeholder accessible manner has attracted much attention from decision-makers (Liang et al., 2015; Wu et al., 2019). Notably, fair RAC allocation is crucial for environmentally and economically harmonious development (Yu et al., 2016; Guo et al., 2021). However, achieving an optimal RAC allocation remains a challenge due to trade-offs between environmental fairness and efficiency (Jiang and Hellegers, 2016; Dai et al., 2018). To address this issue, the environmental Gini coefficient (EGC) has been widely adopted as a method to evaluate the fairness of RAC allocation (Sun et al., 2010; Yu et al., 2016). Characterized by its monotonic properties, the EGC demonstrates that lower values indicate fairer RAC allocations (Yuan et al., 2017; Wang et al., 2021). The EGC integrates environmental capacity with multiple factors, including population, gross domestic product (GDP), land area, livestock numbers, water resources, and other indices (Yuan et al., 2017; Li et al., 2023; Xu et al., 2024). For instance, Sun et al. (2010) selected some socioeconomic indices to calculate the EGC and establish optimal chemical oxygen demand (COD) discharge allocations among 18 county-level divisions in Tianjin, China. Likewise, Yu et al. (2016) combined the EGC with the WASP model to achieve optimal joint control of water quality and quantity in a river watershed based on environmental fairness. Wu et al. (2019) applied the EGC to determine the optimal allocation of ammonia nitrogen ($\text{NH}_3\text{-N}$) discharge permits under different regulatory strategies in the Songhua River Basin. However, the conventional EGC has limitations in its applicability to RAC allocation in river systems. When a river fails to meet its water quality standard, the RAC may exhibit negative theoretical values, leading to the loss of EGC's monotonicity (Li et al., 2023). To avoid this problem, the variable ordering in the objective function is often ignored or treated as a constant, which may not reflect real-world conditions (Wang et al., 2019). Therefore, further modification of the conventional EGC is necessary to improve its rationality and practical

application in RAC allocation.

To address these challenges, the study developed a novel framework for the optimal allocation of RAC by modifying an optimization model based on environmental fairness and efficiency trade-offs. First, RAC was calculated using hydrodynamic and water quality simulations in the MIKE 11 model. Significant factors influencing RAC were identified through an orthogonal experiment, and then different regulatory levels and scenarios were established. To compare the fairness of RAC allocation across scenarios, the EGC was applied. However, the conventional EGC fails to preserve monotonicity under negative RAC values due to theoretical bounds conflicts (e.g., non-negative input requirements) (Wu et al., 2019; Li et al., 2023). To solve this, the EGC was modified with a distribution function. The RAC model was then incorporated into the modified EGC associated with socioeconomic evaluation indices to establish a comprehensive optimization model. The objective function minimized the ratio of the modified EGC variation to the environmental benefit variation of RAC under low, moderate, and high regulatory scenarios, thus optimizing RAC allocation based on fairness-efficiency trade-offs. The framework was applied to the Luan River Basin in Chengde City, China. The study area is crucial for water conservation and ecological protection in the Beijing-Tianjin-Hebei urban agglomeration (Zhao et al., 2020). However, the basin has experienced increasing pressures from excessive pollutant discharges and unsustainable water consumption, posing severe threats to the river environment and socioeconomic sustainability (Tian et al., 2019). Due to the difficulty in considering both fairness and efficiency, the allocation of RAC is still poorly understood. This study supports decision-making for pollutant discharge control and water quality improvement on a watershed scale. The proposed framework is designed to address systemic challenges prevalent in fluvial ecosystems such as assimilative capacity overload, multi-stakeholder conflicts, and limited environmental capacity (Wang et al., 2025). Its design aligns with the globally recognized sustainability paradigm (e.g., UN-Water, 2023), which prioritizes a synergistic balance between environmental fairness and efficiency (Dai et al., 2018; Li et al., 2022).

2. Materials and methods

2.1. Study area

The Luan River Basin in Chengde City ($40^{\circ}12' \text{ N}$ – $42^{\circ}30' \text{ N}$, $115^{\circ}54' \text{ E}$ – $119^{\circ}15' \text{ E}$) is located in Hebei Province, North China (Fig. 1a and b). As the second-largest river in North China, the Luan River is a vital water source for the Beijing-Tianjin-Hebei metropolitan cluster (Zhao et al., 2020). The study area encompasses approximately 64 % of the Luan River Basin and 72 % of Chengde City, covering an area of $2.86 \times 10^4 \text{ km}^2$. This region has a continental monsoonal mountainous climate, with transitions from cold to warm temperatures and from semi-arid to semi-humid conditions. Annual average precipitation is 400–700 mm, with 75 %–85 % concentrated during a short period from June to September. The topography is hilly, with mountains, hills, and basins comprising more than 65 % of the landscape. The terrain slopes downward from northwest to southeast. Agriculture, forest, and grassland are the major land-use types, accounting for over 75 %. Brown and cinnamon soils cover more than 70 % of the area.

According to the Chengde Ecology and Environment Bureau (<https://shj.chengde.gov.cn>), the proportions of primary, secondary, and tertiary industries in 2018 were 18.0 %, 36.3 %, and 45.7 %, respectively. The per capita GDP reached $4.14 \times 10^4 \text{ CNY}$, surpassing the provincial average of $3.60 \times 10^4 \text{ CNY}$ per person. Overall, the GDP, primary, secondary, and tertiary industries showed increasing trends from 1949 to 2018, with average annual growth rates of 8.7 %, 4.4 %, 13.5 %, and 12.2 %, respectively. Rapid urbanization and industrial intensification have significantly increased anthropogenic pollutant discharges into river environments (Tian et al., 2019). To address these pressures, region-specific water quality objectives were established for

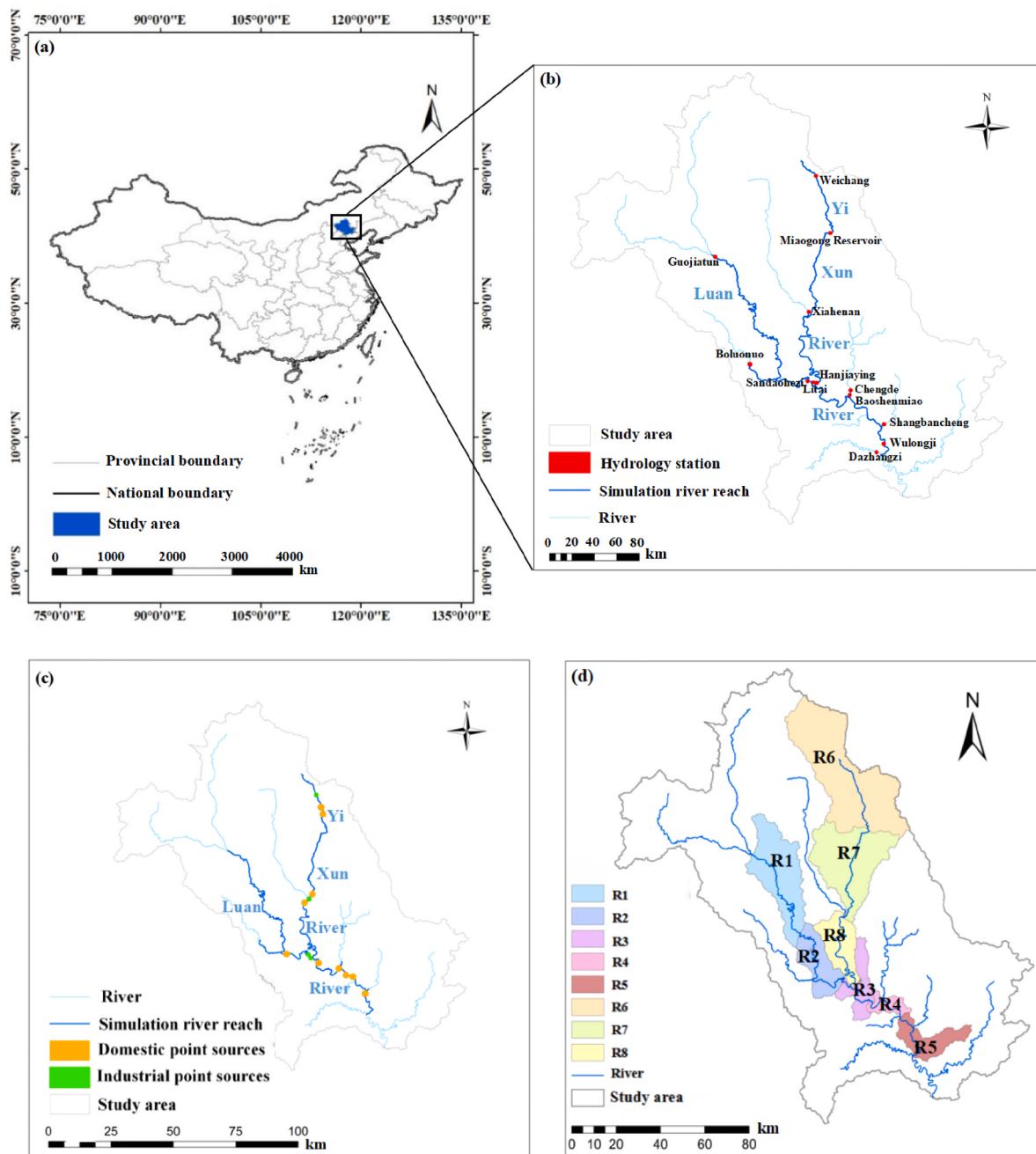


Fig. 1. Maps of the study area. (a) Location; (b) Simulated rivers; (c) Point source pollution distribution; (d) Division of calculation units.

different river sections to meet water environmental management goals. The Luan River and its largest tributary (i.e., Yixun River) have witnessed more intensive socioeconomic activities compared to other tributaries in the basin, leading to higher pollutant discharges primarily categorized as point source pollution (PSP) and non-point source pollution (NPS). Industrial and domestic discharges contributed 20 % and 80 % of PSP, respectively (Chengde Yearbook in 2018). Agricultural activities such as crop cultivation, livestock farming, and fertilizer use could cause NPS, with pollutants entering rivers through processes like soil erosion, rainfall-runoff, and infiltration (Li et al., 2023).

2.2. Overview of the methodological framework

The study area was partitioned into eight calculation units based on water environmental functional zones for RAC assessment. The MIKE 11 model was established to simulate pollutant transport dynamics, with

critical parameters calibrated for RAC calculations. To evaluate the effects of RAC regulation, significant factors influencing RAC were identified through orthogonal experimental design. Four regulatory aspects were selected: domestic point source (DPS), industrial point source (IPS), NPS discharges, and ecological water supply (WS). Regulatory scenarios were defined by adjusting the four aspects to represent varying regulatory levels. For RAC assessment, RAC values were compared across (i) calculation units, (ii) mainstream vs. tributaries, and (iii) different regulatory scenarios. For RAC allocation, the EGC was modified to quantitatively measure the fairness, while the environmental benefit index was applied to reflect the regulatory efficiency. A modified optimization model was then developed using a machine learning approach, balancing fairness and efficiency trade-offs by minimizing an objective function. This function was defined as the minimum ratio of the modified EGC variance to the environmental benefit variance of RAC across different scenarios. The schematic representation of the

framework was illustrated in Fig. 2.

2.3. Process-based MIKE 11 model

2.3.1. Hydrodynamic and water quality modules

The MIKE 11 model, developed by the Danish Hydraulic Institute (DHI), is an internationally recognized tool for simulating

hydrodynamics, water quality, and sediment transport in river systems (DHI, 2003; Talukdar et al., 2023). Considering the geometric and dynamic characteristics of the Luan River Basin, where river length substantially exceeds both the width and depth, the horizontal migration and diffusion of water pollutants along the river flow predominate over vertical and lateral transport processes (Yu et al., 2016). This spatial dynamic of the study area aligns with the one-dimensional modeling

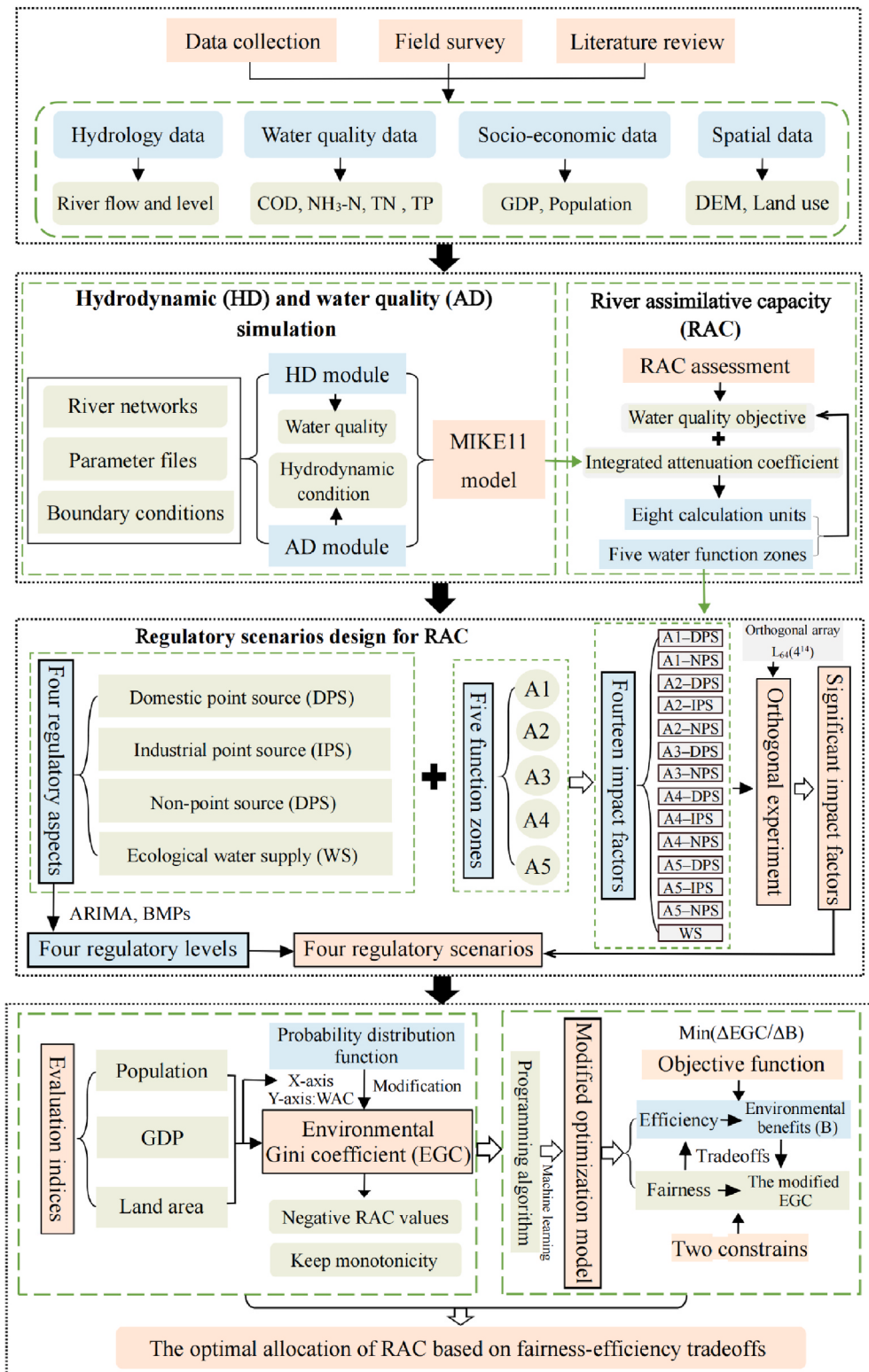


Fig. 2. Schematic diagram of the technological framework.

framework of MIKE 11. A set of modules is embedded into the MIKE 11 model such as rainfall-runoff simulation, hydrodynamic (HD) modeling, and advection-dispersion (AD) analysis (DHI, 2003). In this study, the HD and AD modules were employed for the pollutant transport dynamics. The HD module simulated hydrodynamic conditions essential for quantifying river velocity and flow variations, while the AD module built upon these hydrodynamic outputs to model the spatiotemporal distribution of pollutants (DHI, 2005). By coupling physical transport mechanisms with pollutant degradation processes, the model enabled precise identification of critical control parameters and supported scenario-based optimization of pollution regulation.

The HD module can simulate unsteady flow in river systems using the Saint-Venant equations, which serve as the basis for subsequent water quality simulations (Lafta, 2022). In this study, a 6-point Abbott-Lonescu implicit finite difference scheme was employed. The equations are as follows (Chen et al., 2018):

$$\frac{\partial Q}{\partial x} + \frac{\partial A}{\partial t} = q \quad (1)$$

$$\frac{\partial Q}{\partial t} + \frac{\partial}{\partial x} \left(\alpha \frac{Q^2}{A} \right) + gA \frac{\partial h}{\partial x} + \frac{gQ|Q|}{X^2 AR} = 0 \quad (2)$$

where q is the lateral inflow (m^3/s), x is the distance coordinate (m), t is the time coordinate (s), Q is the river discharge (m^3/s), A is the river cross-section area (m^2), h represents the water level (m), R represents the hydraulic radius (m), g represents gravity acceleration (m^2/s), X is the Chezy coefficient, and α is the momentum distribution coefficient.

Water quality simulations were conducted using the AD module to simulate the migration and degradation of pollutants under various hydrodynamic conditions in aquatic environments (Ji et al., 2022). Water outlets for domestic and industrial pollutant discharges were input into the model as PSP, which were identified as the primary contributors to urban water quality degradation. The spatial distribution of these outlets was obtained from field investigations and document surveys, as shown in Fig. 1c. The NPS data were incorporated into the model using the runoff coefficient method based on rainfall intensities, hydrological runoff processes, and watershed characteristics (Kang et al., 2020). The AD module interfaced with the HD module through a one-dimensional convection-diffusion equation, as follows (Feng et al., 2021):

$$\frac{\partial AC}{\partial t} + \frac{\partial QC}{\partial x} - \frac{\partial}{\partial x} \left(AD \frac{\partial C}{\partial x} \right) = -AKC + C_2 q \quad (3)$$

where C is the water quality concentration (mg/L), D is the river's longitudinal diffusion coefficient (m^2/s), K is the linear attenuation coefficient of pollutants ($1/\text{d}$), and C_2 is the concentration at the pollutant source/sink (mg/L).

2.3.2. Data acquisition and preparation

The MIKE 11 model integrates multiple datasets to establish a coupled hydrodynamic and water quality simulation system. The datasets required for the MIKE11 model include topological, meteorological, hydrological, and water quality data, as summarized in Table S1. Topological data were derived from the SRTM DEM with a spatial resolution of $30 \text{ m} \times 30 \text{ m}$ (Geospatial Data Cloud Platform). Meteorological inputs included daily precipitation, evaporation, and wind speed data with a 1-day time step, which were sourced from the Chengde Meteorological Bureau. Hydrological boundary conditions were defined using daily river discharge and water level data, monitored by the Hydrographic and Water Resources Survey Bureau. These datasets were organized into five essential input files—including river network configurations, cross-sectional data, boundary conditions, time-series inputs, and parameter specifications—to establish HD module of the study area (DHI, 2005).

The AD module relied on flow fields generated by the HD module to simulate pollutant transport. Additional datasets were input into the AD module, including water quality parameters (WQPs), pollution sources, pollutant initial conditions. According to the 2018 Environmental Quality Report of Chengde City, eight WQIs—including dissolved oxygen, permanganate index, biochemical oxygen demand, petroleum, COD, $\text{NH}_3\text{-N}$, total nitrogen (TN), and total phosphorus (TP)—were evaluated at six water quality stations (i.e., Guojiatun, Wulongji, Weichang, Litai, Baoshenmiao, and Dazhangzi stations), as shown in Fig. 1b. Therein, COD, $\text{NH}_3\text{-N}$, TN, and TP were identified as the most critical WQPs in the river basin, with the discharge amounts of 5.42×10^6 , 2.20×10^6 , 3.88×10^6 and $1.93 \times 10^5 \text{ kg}$ in 2018, respectively. Therefore, the four critical WQPs were selected as primary simulation targets, with pollutant sources categorized into PSP and NPS. Point source data, such as spatial coordinates and emission rates (Fig. 1d), were incorporated into the model as boundary conditions, while non-point sources were estimated using a river input coefficient method. Furthermore, the MIKE 11 model required the generalization of river networks and the extraction of major rivers (DHI, 2003). The primary river (i.e., Luan River) and its largest tributary (i.e., Yixun River) were identified as the most polluted rivers and therefore selected for simulation.

2.3.3. Model calibration and verification

The calibration and verification periods for the HD and AD modules were established based on their module-specific data requirements and modeling objectives. The HD calibration required continuous river discharge data spanning complete hydrological cycles to characterize seasonal flow variations and extreme events (Talukdar et al., 2023). This process involved iterative adjustment of Manning's roughness coefficient, with performance evaluated using the Nash-Sutcliffe efficiency (NSE) and mean absolute percentage error (MAPE). In contrast, the AD module needed high-frequency pollutant concentration sampling during dry/rainy seasons to quantify pollutant transport dynamics. Parameter optimization targeted the longitudinal diffusion coefficient (D) and integrated attenuation coefficient (K), with accuracy quantified by the relative error (RE) between simulated and measured concentrations.

In the HD module, measured daily river discharge data from the Litai and Wulongji stations were used for calibration from 1 January 2010 to 31 December 2010, with verification from 1 January 2015 to 31 December 2015. The simulation time step was 60 s. The HD calibration served as a prerequisite for the AD module calibration. The AD module was initially operated with default settings, which were subsequently refined by calibrating D and K . The AD calibration utilized measured pollutant concentration data from 1 January to 30 June 2018, with verification conducted from 1 July to 31 December 2018. Model performance was evaluated using the NSE, MAPE, and RE (Lamontagne et al., 2020; Bui and Pham, 2023). The formulas are as follows (Ji et al., 2022):

$$NSE = 1 - \frac{\sum_{t=1}^n (C_m - C_s)^2}{\sum_{t=1}^n (C_m - \bar{C})^2} \quad (4)$$

$$MAPE = \sum_{t=1}^n \left| \frac{C_m - C_s}{C_s} \right| \times \frac{100}{n} \quad (5)$$

$$RE = \frac{|C_s - C_m|}{C_m} \times 100\% \quad (6)$$

where C_m and C_s are the measured and simulated values at time t for the four WQPs concentrations, respectively. \bar{C} represents the average of all measured values for the WQP concentrations, and n is the total number of WQPs. The model's reliability and accuracy improve as the NSE and MAPE approach 1. Furthermore, a RE closer to 0 indicates better agreement between the simulated and measured values (DHI, 2003;

Lafta, 2022).

2.4. River assimilative capacity (RAC) calculation

2.4.1. Division of calculation units

The RAC assessment was based on water calculation units. However, delineating calculation units based solely on the traditional administrative division method has been criticized (Wu et al., 2019; Xie et al., 2022). This was because pollutant discharges were unlikely to affect areas outside the watershed, despite being within the same administrative county. To address this limitation, this study combined both basin characteristics and administrative boundaries to determine the calculation units. First, watershed boundaries were derived using the ArcGIS Hydrological Toolbox (v10.8) with a depressionless DEM. Next, hydrological response units were delineated based on the geographical location, topography, land use, soil properties, and meteorological characteristics. These sub-basins units were then overlaid with pollutant discharge points, monitoring cross-sections, and county-level administrative boundaries to divide the study area into eight calculation units (Fig. 1d). This dual-criteria approach reconciles watershed dynamics with administrative regulation (Wu et al., 2019; Bui and Pham, 2023).

2.4.2. Water quality objectives

Determining the specific water quality objective for each calculation unit is essential for RAC calculations. The water environmental function zone is the primary reference for determining the targeted water quality objective (Li et al., 2023). This is based on dominant functions in accordance with socioeconomic conditions, projected development plans, water resources utilization strategies, and eco-environmental preservation requirements (Yan et al., 2012; Kang et al., 2020). Guided by China's three-level water ecological environment zoning management system (MEE, 2016) and the Hebei Province Water Function Zoning regulations (Water Resources Document [2017] No. 127), the study area was divided into five water environmental function zones. The corresponding water quality objectives for each calculation unit were then identified, as shown in Table 1.

2.4.3. Calculation of RAC

The water quality objective and the K were the primary variables to calculate RAC. The K represented the combined effects of pollutant degradation and environmental factors, which was critical for quantifying self-purification capacity (M_s) and was calibrated using field data (DHI, 2003; Talukdar et al., 2023). Based on the established HD and AD modules, the process-based MIKE 11 model for simulating pollutant generation-diffusion-transfer dynamics was established, identifying the critical parameter K for RAC calculations (Zhao et al., 2018). For regulated rivers, the water quality standards (S) conformed to China's

Environmental Quality Standards for Surface Water (GB 3838-2002), which defined the target concentration thresholds for COD, $\text{NH}_3\text{-N}$, TN, and TP that determined whether a calculation unit had residual assimilative capacity (Chen et al., 2014). The formulas are as follows (CAEP, 2003):

$$M_i = M_s + M_d \quad (7)$$

$$M_s = 86.4 \times S Q_t \left(1 - e^{-\frac{KL}{86400v}} \right) \quad (8)$$

$$M_d = 86.4 \times (S - C_b) \times Q_r \quad (9)$$

$$M_{r(i)} = (1 - p_i) \times M_{0(i)} \quad (10)$$

where M_i is the RAC for the i th calculation unit (kg/d), M_s is the self-purification capacity (kg/d), M_d is the dilution capacity (kg/d), $M_{r(i)}$ is the RAC after regulation for the i th unit (kg/d), S represents the water quality standard (mg/L), Q_t is the total of river flow and wastewater discharge (m^3/s), L is the river length (m), K is the integrated attenuation coefficient (1/d), v is the river velocity (m/s), C_b is the river background concentration (mg/L), Q_r is the river discharge (m^3/s), p_i is the regulatory level for the i th unit (%), and $M_{0(i)}$ is the RAC at the initial state (kg/d).

According to the formulas, the RAC value is non-positive ($M_i \leq 0$) when the water quality does not meet the specified standards, indicating that the river section lacks the residual capacity to assimilate pollutant loads (Chen et al., 2014; Li et al., 2023). When C_b exceeds S ($C_b \geq S$), it indicates that legacy contamination has saturated the river self-purification capacity. When the ratio of river discharge to the integrated attenuation coefficient (Q_r/K) drops under required levels, it reflects insufficient hydrodynamic dispersion or biochemical degradation capacity. Negative RAC ($M_i \leq 0$) occurs when $C_b \geq S$ or Q_r/K falls below critical thresholds, necessitating regulatory intervention.

2.5. Regulatory scenarios design

2.5.1. Contributing factors on RAC

The RAC allocation is defined as the distribution among different sectors (Hu et al., 2016). Domestic, industrial, agricultural, and ecological water uses constitute four fundamental sectors of water resources management (Zhu et al., 2022). The study area suffered from two major water resources challenges—freshwater shortages and water pollution. Specifically, per capita water resources in Chengde City were $987 \text{ m}^3/\text{person/year}$ (Chen et al., 2018), which was below the internationally recognized threshold for water scarcity of $1000 \text{ m}^3/\text{person/year}$. Seasonal variations in runoff were observed, with precipitation from June to September accounting for 75%–85% of the annual total.

Table 1

Basic information on the five water environmental function zones and the eight calculation units.

Function zone	Function zone division	Calculation unit	Calculation unit division (start-end hydrology station)	River	Land area (km^2)	Total population	GDP (10^5 CNY)	Population density (person/ km^2)	Water quality objective
A1	Luan River–Chengde reservation zone	R1	Guojiatun–Xinglongzhuang	Luan	1117	77103	24482	69	III
		R2	Xinglongzhuang–Sandaohizi	Luan	564	55295	27121	98	III
A2	Luan River–Chengde development and utilization zone I	R3	Sandaohizi–Shimenzi	Luan	395	138568	116526	351	III
		R4	Shimenzi–Shangbancheng	Luan	186	130953	58212	703	III
A3	Luan River–Chengde development and Utilization zone II	R5	Shangbancheng–Wulongji	Luan	440	47362	15023	108	III
A4	Yixun River–Chengde water source conservation zone	R6	End of Yixun River–Miaogong Reservoir	Yixun	2176	102945	31908	47	II
A5	Yixun River–Chengde development and utilization zone	R7	Miaogong Reservoir–Maocilu Village	Yixun	1524	105146	34091	69	III
		R8	Maocilu Village–Hanjiaying	Yixun	319	35757	20948	112	III

The construction and operation of multiple reservoirs (e.g., Miaogong, Panjiakou, and Daheiting Reservoirs) and water conservancy projects had a significant influence on the river flow discharge and velocity, thus changing the migration and transformation of pollutants (Yan et al., 2012; Tian et al., 2019). Moreover, large volumes of polluted water from agricultural, industrial, and domestic sources were discharged into the river, resulting in higher concentrations of some WQPs. Therefore, four regulatory aspects were considered to reduce pollutant discharges and improve water quality, including decreases in DPS, IPS, NPS, and an increase in WS. Consequently, by combining with the five water environment function zones (i.e., A1, A2, A3, A4 and A5) in the river basin, fourteen impact factors were identified. These factors included A1–DPS, A1–NPS, A2–DPS, A2–IPS, A2–NPS, A3–DPS, A3–NPS, A4–DPS, A4–IPS, A4–NPS, A5–DPS, A5–IPS, A5–NPS, and WS.

2.5.2. Orthogonal experiment

To assess the influence of multiple factors on the RAC of four WQPs in eight calculation units, it is necessary to consider every possible combination of all contributing factors. A complete multi-factor scheme using an exhaustive method with k factors at p levels would require p^k tests (Gan et al., 2014). However, as the number and levels of factors increase, the experimental complexity grows geometrically, potentially exceeding the capacity of decision-making systems. To address this challenge, an orthogonal experiment was employed to identify which factors and their interactions significantly influenced RAC in this study, thereby improving efficiency and providing high-quality data for decision-making (Guo et al., 2019). Specifically, an orthogonal array was used to determine representative combinations of all contributing factors, effectively reducing the number of experiments (Wu and Hamada, 2009). This method guaranteed uniform testing frequency for all factor levels within the orthogonal design while preserving statistical independence between factors, thereby enabling isolation of individual factor effects and their interactions (Gan et al., 2014). The significance of contributing factors on RAC was assessed through analysis of variance (ANOVA) using F -value and p -value. A higher F -value indicated a greater influence, while the p -value was tested at a 95 % confidence level.

2.5.3. Setting of regulatory levels

Several scenarios with different regulatory levels were analyzed to compare RAC allocations. The regulatory levels of point source pollution in Chengde City were determined to use the Autoregressive Integrated Moving Average (ARIMA) model. ARIMA is a widely used univariate statistical analysis technique that combines autoregression (p), differencing (d), and moving average (q) (Arora and Keshari, 2021). This model can effectively handle time series data to forecast future values, and has been widely applied in water resources management, such as water quality prediction (Bi et al., 2021). In this study, the ARIMA model was applied to forecast the reduction rates of DPS and IPS in eight calculation units. By inputting historical annual concentration data of COD, NH₃-N, TN, and TP discharges, the model generated reduction rate predictions for 2019. Specifically, stationarity tests were performed on the WQP concentration time series from 2011 to 2018. The ARIMA model parameters (p, d, q) were initially determined by analyzing the stationarity of hydrological data through the autocorrelation function and the partial autocorrelation function of time-series data of water quality (Box et al., 2015). The parameters were then optimized via maximum likelihood estimation to minimize the Akaike Information Criterion (AIC). The model with the lowest AIC was selected to balance goodness-of-fit and complexity (Hyndman and Athanasopoulos, 2018). The model stability was verified by 95 % confidence intervals (CIs). These intervals could quantify the uncertainty associated with the point estimates, reflecting the statistical reliability of the forecasts (Bi et al., 2021). The CI bounds directly defined the minimum and maximum feasible reduction rates under each regulatory level.

The regulation of non-point source pollution is based on the TMDL model proposed by the U.S. Environmental Protection Agency (Qin

et al., 2013; Rai et al., 2024). Its core principle involves quantifying the maximum assimilative capacity of water bodies for pollutants through mathematical methods. Unlike traditional measures that focus solely on effluent discharge standards, TMDL adopts a watershed-based approach integrating pollutant reduction targets and RAC allocations (Sado et al., 2010; Wang et al., 2024). Best management practices (BMPs) play a crucial role in achieving the TMDL requirements to reduce NPS and improve water quality (Qin et al., 2013; Wang et al., 2025). In this study, the BMPs were selected based on the Luan River Basin's dominant land-use types (e.g., 45 % agriculture, 18 % forest), soil properties (i.e., silty loam with high erodibility), and seasonal flow dynamics (i.e., peak discharge in July–September). Therefore, regulatory levels for NPS were designed based on region-specific BMPs.

2.6. Optimal allocation of RAC

2.6.1. The modified environmental economic model

The fairness-based allocation of RAC requires quantifiable method. In this study, the Gini coefficient was applied as a dual-objective fairness indicator proposed by the Italian economist Corrado Gini (1936), which was widely extended in water resources and environmental management (Wu et al., 2019; Zhang et al., 2023). The environmental Gini coefficient generalizes the cumulative percentage of income on the vertical axis to represent assimilative capacity or pollutant discharges (Yuan et al., 2017; Shu and Xiong, 2018), while the cumulative percentage of population on the horizontal axis corresponds to the relevant evaluation index (Li et al., 2023), as shown in Fig. 3a and b. In this study, the X-axis represented the evaluation index, and the Y-axis represented the RAC. Similar to the data sorting method of the traditional Gini coefficient based on ascending order of income (Yuan et al., 2017), the RAC for each calculation unit under each evaluation index was systematically arranged in ascending order for the four studied WQPs. The EGC is calculated using the Lorenz curve and the trapezoidal rule, as follows (Wu et al., 2019):

$$G_j = 1 - \sum_{i=1}^n (X_{ij} - X_{(i-1)j})(Y_i + Y_{i-1}) \quad (11)$$

where G_j represents the EGC value, j is one of the evaluation indices of the EGC, i is the ordinal number of the RAC in calculation units, X_{ij} is the cumulative percentage of the j th evaluation index in the i th unit, and Y_i is the accumulative percentage of the RAC in the i th unit. A smaller EGC value indicates a fairer allocation of RAC (Yu et al., 2016).

The Lorenz curve lies in the first quadrant with both horizontal and vertical coordinate values being positive. However, the RAC values become negative when water quality fails to meet the targeted objective according to Formula (9), causing a loss of monotonicity in EGC, which violates the property that a lower Gini coefficient corresponds to greater fairness (Zhao et al., 2018). When the variable Y (e.g., RAC) contains negative values but maintains a positive mean, the initial segment of the Lorenz curve lies below the X-axis, resulting in an EGC value exceeding 1 ($G > 1$) (Fig. 3c). If Y has both negative values and a negative mean, the Lorenz curve shifts above the line of perfect equality, yielding a negative EGC (Fig. 3d). In this case, the EGC model becomes ineffective for evaluating the fairness of RAC allocations (Yuan et al., 2017; Zhang et al., 2023). To address this issue, this study modified the conventional EGC by incorporating a probability distribution function to overcome the loss of non-monotonicity due to negative RACs. All possible values of RACs were categorized into negative (NRAC), zero (ZRAC), and positive (PRAC) river assimilative capacities within the piecewise distribution functions. Mathematically, the formulas are as follows:

$$G(x) = \begin{cases} q_1 G_1(x), & x < 0 \\ 1 - q_2, & x = 0 \\ 1 - q_2 + q_2 G_2(x), & x > 0 \end{cases} \quad (12)$$

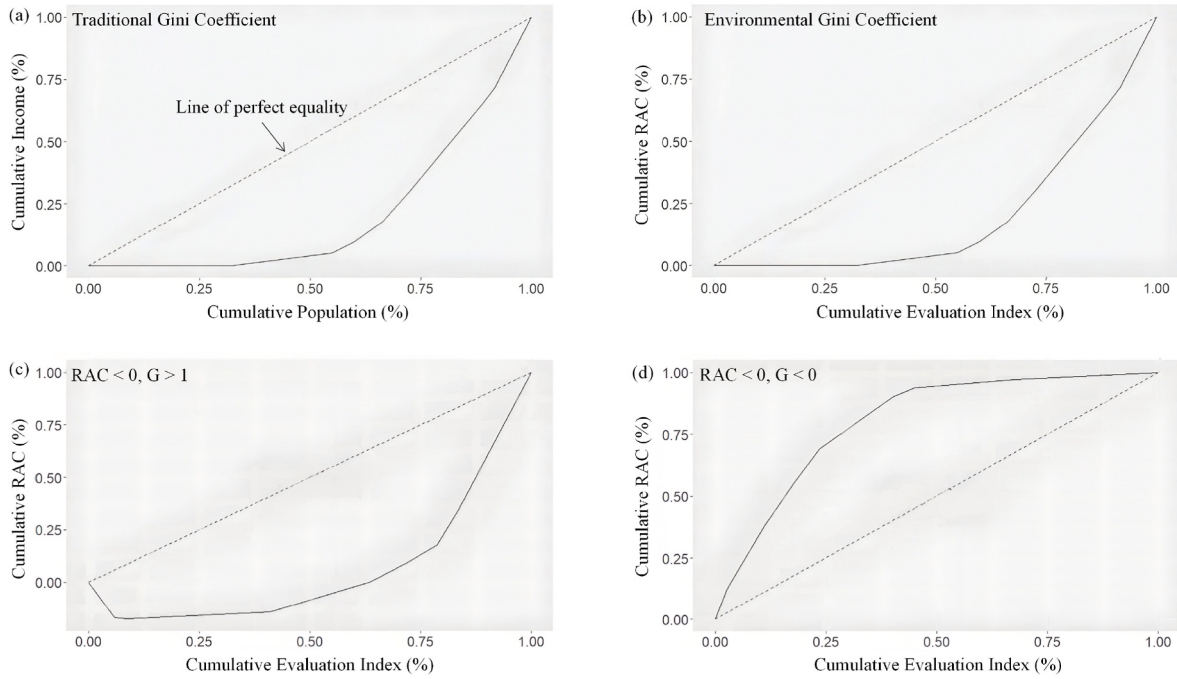


Fig. 3. Lorenz Curve. (a) Traditional Gini coefficient; (b) Environmental Gini coefficient (EGC); (c) EGC with negative RAC values but positive overall mean; (d) EGC with negative RAC values and negative overall mean.

$$G_1(x) = \int_{\min}^x g_1(t) dt \quad (13)$$

$$G_2(x) = \int_0^x g_2(t) dt \quad (14)$$

where q_1 and q_2 are the proportions of NRAC and PRAC, respectively. $G_1(x)$ and $G_2(x)$ are the distribution functions of NRAC and PRAC, respectively. Additionally, $g_1(x)$ and $g_2(x)$ represent the probability density functions of NRAC and PRAC, respectively.

The EGCS for the NRAC (G_1) and PRAC (G_2) are obtained using the integral method, as follows:

$$G_1 = \int_{\min}^0 G_1(x)(1 - G_1(x)) dx / |\mu_1| \quad (15)$$

$$G_2 = \int_0^{\max} F_2(x)(1 - G_2(x)) dx / \mu_2 \quad (16)$$

where μ_1 and μ_2 represent the average value of NRAC and PRAC, respectively.

The EGC is 0 since all values of ZRAC in each calculation unit are the same. Therefore, the modified EGC for the RAC is calculated as follows:

$$G = \int_{\min}^{\max} G(x)(1 - G(x)) dx / \mu = \int_{\min}^0 G(x)(1 - G(x)) dx / \mu + \int_0^{\max} G(x)(1 - G(x)) dx / \mu \quad (17)$$

Then Formula (17) is simplified as follows:

$$\int_{\min}^0 G(x)(1 - G(x)) dx$$

$$G = \int_{\min}^0 q_1 G_1(x)(1 - q_1 G_1(x)) dx$$

$$= \int_{\min}^0 q_1 G_1(x)(q_1 - q_1 G_1(x) + 1 - q_1) dx$$

$$= q_1^2 \int_{\min}^0 G_1(x)(1 - G_1(x)) dx + q_1(1 - q_1) \int_{\min}^0 G_1(x) dx$$

$$= q_1^2 |\mu_1| N_1 + q_1(1 - q_1) |\mu_1| \quad (18)$$

$$\int_0^{\max} G(x)(1 - G(x)) dx$$

$$= \int_0^{\max} (1 - q_2 + q_2 G_2(x))(q_2 - q_2 G_2(x)) dx$$

$$= q_2^2 \int_0^{\max} G_2(x)(1 - G_2(x)) dx + q_2(1 - q_2) \int_0^{\max} (1 - G_2(x)) dx$$

$$= q_2^2 \mu_2 N_2 + q_2(1 - q_2) \mu_2 \quad (19)$$

After simplification, the modified EGC model can be expressed as follows:

$$G = [q_1^2 |\mu_1| G_1 + q_1(1 - q_1) |\mu_1|] / \mu + [q_2^2 |\mu_2| G_2 + q_2(1 - q_2) |\mu_2|] / \mu$$

$$= q_1^2 \frac{|\mu_1|}{\mu} G_1 + q_2^2 \frac{|\mu_2|}{\mu} G_2 + q_1(1 - q_1) \frac{|\mu_1|}{\mu} + q_2(1 - q_2) \frac{|\mu_2|}{\mu} \quad (20)$$

2.6.2. The modified optimization model

The framework of RAC allocation was designed to balance fairness and efficiency through a constrained multi-objective optimization model. The optimization objective was formally defined as minimizing the trade-off between fairness degradation and environmental benefits across eight calculation units. The fairness of RAC allocation was evaluated using the modified EGC, which facilitated opportunities for underdeveloped subareas and reduced conflicts between cost and fairness (Yuan et al., 2017; Shu and Xiong, 2018). However, overemphasis on fairness may lead to inefficiencies, as it could restrict permissible pollutant discharges to meet diverse development needs of different calculation units (Hu et al., 2016; Li et al., 2022). In practice, regulatory agencies often impose environmental taxes to promote efficiency, which serve as an important environmental management tool (Zhang et al., 2018). It is directly linked to pollutant discharge amounts,

concentrations, and types, which can reflect the environmental benefits. The formula is expressed as follows:

$$\Delta B = \frac{M_{r(i)} - M_{0(i)}}{M_{0(i)}} \times F_{WQP} \quad (21)$$

where ΔB represents the change value of environmental benefits under different regulatory scenarios, and F_{WQP} represents the pollutant discharge fee for the WQP (CNY/kg).

The RAC allocation based on fairness-efficiency trade-offs considered environmental benefits while ensuring balance among subareas (Wu et al., 2022). The modified EGC quantitatively assessed the fairness of RAC allocation, while the environmental benefits mathematically measured its efficiency. The optimal allocation was determined by an objective function and two constraints. The objective function aimed at minimizing the ratio of the modified EGC change (ΔG_j) to the environmental benefit change (ΔB) under different scenarios, as follows:

$$\min \left(\frac{1}{n} \sum_{j=1}^n \frac{\Delta G_j}{\Delta B} \right) \quad (22)$$

The two constraints of the optimal allocation were: (a) The RAC was within the upper and lower bounds for pollutant regulatory rates in eight calculation units. (b) The modified EGC for each evaluation index remained below its initial state. The formulas are as follows:

$$\begin{cases} M_i^{\min} < M_i < M_i^{\max} \\ G_j < G_{j(0)} \end{cases} \quad (23)$$

where M_i is the RAC in the i th unit, and M_i^{\min} and M_i^{\max} correspond to the lower and upper limits of the RAC after regulation in the i th calculation unit, respectively. $G_{j(0)}$ is the baseline EGC at the initial state.

Given that the modified EGC was calculated based on RAC values in eight calculation units ranging from the minimum to the maximum value, the objective function could not be expressed using elementary functions of the original variables due to the involvement of order statistics (Xie et al., 2018; Feng et al., 2021). Previous research often assumed that the RAC sequence for each calculation unit remained fixed, thus regarding the EGC as an elementary function for optimization problems (Yu et al., 2016; Wang et al., 2019). This study adopted a grid search optimization method from machine learning to address the limitations of conventional algorithms in solving programming equations involving order statistics. This approach systematically identifies the optimal combination of hyperparameters by exhaustively searching through a specified subset of the parameter grid. In this study, a reasonable step size was chosen to construct a grid of all possible RAC values for each calculation unit, ranging from the minimum to maximum value. This process established all possible combinations of RAC values across all calculation units. The optimized grid search step sizes (COD = 100 kg/d, NH₃-N = 10 kg/d, TN = 50 kg/d, TP = 1 kg/d) balanced computational efficiency (>95 % convergence) with accuracy (errors <1 %), in compliance with China's *Technical Guidelines for Environmental Impact Assessment—Surface Water Environment* (HJ 2.3–2018). The combination that minimized the objective function within the constraints was then identified as the optimal RAC allocation strategy.

3. Results and discussion

3.1. Three regulatory scenarios for RAC

3.1.1. Orthogonal experimental outcomes

Comprehensive consideration of contributing factors for RAC is crucial for improving water quality). While increasing the number of variables can enhance model accuracy, it also risks introducing computational redundancy, particularly when certain variables exhibit minimal contributions to output variance (Gan et al., 2014). Therefore,

identifying significant contributing factors for RAC is essential for setting regulatory levels. In this study, an orthogonal array L₆₄ (4¹⁴) was used to evaluate 14 experimental factors across 4 regulatory aspects (Table S2). The orthogonal experimental design effectively eliminated redundant factors and identified key contributors. The significance of each factor on the RAC of WQPs in each calculation unit was assessed using *F*-tests and *p*-values, with the results shown in Table S3–S10.

The RACs of the four studied WQPs in R₁ were predominantly influenced by A1–NPS (*p* < 0.01), indicating that regulating NSP was a key strategy for controlling pollutant discharges (Table S3). In R₂, the RACs for COD, NH₃-N, and TN were mainly impacted by both A1–DPS and A1–NSP, while the RAC_{TP} was primarily influenced by A1–NPS (*p* < 0.01). Specifically, the RACs for COD and NH₃-N in R₂ were more sensitive to PSP, while the RACs for TN and TP were notably affected by NSP, with the highest *F*-values of 906.26 and 76.90, respectively (Table S4). For R₃, the significant contributing factors for the RAC_{COD} were A2–DPS, A2–IPS and A1–DPS, with highest *F*-values of 3202.77, 1261.37, and 1029.37, respectively (Table S5), indicating the importance of reducing A2–DPS to improve RAC_{COD} in R₃. The WS from the Miaogong Reservoir played a pivotal role in increasing RAC_{NH3-N} at the R₃ river confluence. This was mainly because the regulation of the Miaogong reservoir altered water volume and hydrodynamic conditions, releasing previously intercepted sediments and nutrients into R₃. This process was amplified by the backwater effect at the confluence of the tributary and mainstream. For TP in R₃, improvements in RAC were most associated with reductions in A1–NPS, followed by A5–NPS. This effect was attributed to the extensive agricultural activities upstream in the Luan River (R₁ and R₂) and Yixun River (R₇ and R₈), where NSP control measures not only enhanced local RAC but also positively influenced downstream areas like R₃. In R₄, RAC_{COD} was primarily affected by A2–DPS, A2–IPS, and A1–DPS, while regulation of A2–DPS significantly influenced RAC_{NH3-N} (Table S6). Additionally, A1–NPS, A2–APS, and A2–DPS had marked effects on the RACs for TN and TP in R₄. In R₅, RACs for COD and NH₃-N were primarily dominated by A2–DPS and A3–DPS (Table S7). RAC_{TN} was influenced by A3–NPS and A3–DPS, whereas RAC_{TP} was driven by A1–NPS and A3–NPS.

Along the Yixun River, the RACs for COD and NH₃-N in R₆ increased with reductions in A4–DPS (Table S8). Significant contributing factors for RAC_{TN} included A4–DPS, A4–NPS, A5–NPS, and WS. However, A6–NPS and WS had no significant impact. This was because A₅ and the Miaogong Reservoir were located downstream of R₆, and downstream regulatory measures did not affect the upstream RAC. For RAC_{TP}, A4–NPS was the only significant factor. In R₇ and R₈, the RACs for COD and NH₃-N were influenced by A5–DPS and A5–IPS, with peak values of 601.26 and 232.84 for COD, and 4.58 and 1.37 for NH₃-N, respectively (Table S9 and Table S10). Additionally, A5–NPS and A5–DPS were identified as significant contributing factors for RAC_{TN}, while the RAC_{TP} was dominated by A5–NPS and WS. Overall, the significance of each contributing factor is shown in Table 2.

3.1.2. Setting of three regulatory levels

Using the annual total discharges of COD, NH₃-N, TN, and TP from point source pollution during 2011–2018, as reported in Chengde Statistical Yearbook, the ARIMA model was applied to predict the regulatory levels of DPS and IPS. The autocorrelation function exhibited exponential decay after lag 1, while the partial autocorrelation function truncated at lag 1. To address uncertainty in visual interpretation, a grid search was performed over $p \in \{0, 1, 2\}$ and $q \in \{0, 1, 2\}$. The differencing order d was fixed at 1, since the stationarity was confirmed by the Augmented Dickey-Fuller test (*p* < 0.05). For the Luanhe Basin water quality series, the ARIMA(1, 1, 1) model achieved the lowest AIC (305.21), demonstrating an optimal balance between accuracy and simplicity. Table S11 showed the results of predicted reduction rates and their CIs for domestic and industrial discharges of COD, NH₃-N, TN, and TP, categorizing reduction rates into three regulatory levels (1, 2, and 3) for each water environmental function zone. Table 3 displays the

Table 2

Orthogonal experiment results of significant factors on RAC in each calculation unit (* $P < 0.05$, ** $P < 0.01$). Blue blocks present DPS, gray blocks present IPS, red blocks present NPS, and green blocks present WS (hereinafter the same).

	A1-DPS	A1-NPS	A2-DPS	A2-IPS	A2-NPS	A3-DPS	A3-NPS	A4-DPS	A4-IPS	A4-NPS	A5-DPS	A5-IPS	A5-NPS	WS
R1		**		*		*								
R2	**	**					*							
R3	**	**	**	**	**		*			*	*	*		**
R4	**	**	**	**	**				*					**
R5		**	**	**	**	**	**	*						
R6								**	**	**			**	*
R7		*						**	*	**		**	**	**
R8			*					*		**		**	**	**

regulatory levels and scenarios for the four WQPs from DPS and IPS. Level 0 served as the baseline scenario, maintaining current pollution discharge levels with 0 % reduction. Level 2 represented moderate regulatory level, adopting predicted median reduction rates: DPS achieved reduction rates of 34.762 % (COD), 23.143 % (NH₃-N), 15.659 % (TN), and 18.793 % (TP), while IPS attained 27.735 % (COD), 22.586 % (NH₃-N), 14.842 % (TN), and 16.269 % (TP). Level 1, defined by the lower CIs, enforced conservative targets with DPS reduction rates of 24.526 % (COD), 16.929 % (NH₃-N), 10.446 % (TN), and 13.665 % (TP), and IPS reduction rates of 20.207 % (COD), 16.421 % (NH₃-N), 11.021 % (TN), and 11.510 % (TP). Level 4, aligned with the upper CIs, implemented higher regulation requiring DPS reductions rates of 44.996 % (COD), 29.357 % (NH₃-N), 20.872 % (TN), and 23.921 % (TP), alongside IPS reduction rates of 35.263 % (COD), 28.751 % (NH₃-N), 18.663 % (TN), and 21.028 % (TP).

Previous studies showed that integrated watershed management measures could significantly reduce pollutant discharges from NPS of COD, NH₃-N, TN, and TP by 9%–60%, 20%–47%, 7%–34% and 13%–36%, respectively (Sun et al., 2013a; Taylor et al., 2016; Zhao et al., 2020). In practice, the study analyzed regulatory levels for NPS pollution reduction by considering agricultural cultivation methods, fertilizer and pesticide use, and policies interventions. The study area implemented various BMPs, such as reducing fertilizer use, refining fertilizer compositions, promoting soil and water conservation, and establishing vegetation buffer zones. For example, vegetated buffer strips planted with *Phragmites australis* and *Tamarix chinensis* in agricultural sub-basins with slopes >10° reduced TN and TP runoff by 10–30 % through sediment trapping and nutrient uptake (Chengde Ecology and Environment Bureau). Controlled fertilization measures implemented in corn-dominated zones mitigated nitrogen surplus by 10–30 % via optimized nitrogen-phosphorus-potassium ratios and real-time soil nutrient sensors (Chengde Agriculture Bureau). Constructed wetlands installed downstream of agricultural zones enhanced phosphorus retention by 10–30 % during peak discharge months via biofiltration and adsorption (Hebei Provincial Government). Based on these region-specific BMPs, three reduction levels were established for NPS pollution reduction (Table 3 and Table S12). Reduction rates of 10%, 20%, and 30% for the four WQPs were assigned to regulatory Levels 1, 2, and 3, respectively. Level 0 served as the baseline.

Regarding WS, the Miaogong Reservoir played a vital role in alleviating water supply conflicts and mitigating water environmental pollution in the study area (Tian et al., 2019). The reservoir was a large comprehensive water diversion project, with a total storage capacity of $1.83 \times 10^8 \text{ m}^3$ and an average annual runoff of $1.2 \times 10^8 \text{ m}^3$. Moreover, it serviced an irrigation area of $4.3 \times 10^7 \text{ m}^2$, providing an annual irrigation water supply of $8.59 \times 10^7 \text{ m}^3$ (Liu et al., 2016). In addition,

the Miaogong Reservoir made a difference to the RACs in more than half of the area. Therefore, WS was identified as one of the most important regulatory aspects. Specifically, Level 0 preserved the baseline WS volumes, while Levels 1–3 progressively increase inflow by 2%, 4%, and 6%, respectively.

Overall, for PSP and NPS reduction, the baseline scenario (0 % reduction) was set as Level 0 for reference. Level 2 represented the predicted reduction rate based on model outputs, while Levels 1 and 3 corresponded to the lower and upper confidence intervals of the predicted reduction rate, respectively. For WS, the initial state (0 % increase) was set as Level 0, with increases of 2%, 4%, and 6% in water inflow corresponding to Levels 1, 2 and 3, respectively. As shown in Table 3, Levels 1, 2, and 3—corresponding to low, moderate, and high regulatory scenarios, respectively—were defined for four WQPs (i.e., COD, NH₃-N, TN, TP) across four regulatory aspects (i.e., DPS, IPS, NPS, and WS). Level 0 was set as the baseline scenario reflecting the status quo.

3.2. River assimilative capacity assessment

3.2.1. Parameters for RAC calculations

Hydrodynamic and water quality simulations were performed to identify the key parameters for RAC calculations. In the AD module, the Manning's roughness coefficients ranged from 0.022 to 0.054 m/s^{1/3} for the Luan River and from 0.024 to 0.061 m/s^{1/3} for the Yixun River. The NSE and MAPE values for the Wulongji station were 0.66 and 27 % during calibration, and 0.61 and 35 % during verification, respectively (Fig. S1). Both the NSE (>0.6) and MAPE (<36 %) values demonstrated that the model performance was acceptable for simulating hydrodynamic processes and reliable for subsequent water quality simulations (Moriasi et al., 2007; Lamontagne et al., 2020).

The AD module required calibration for critical parameters, including the D and K of pollutant discharges (Zhao et al., 2018; Ji et al., 2022). These parameters were adjusted based on measured concentrations of WQPs in the river monitoring sections (DHI, 2003), and then incorporated into the RAC model Table 4 presented the K values for each WQP, which quantified the river self-purification capacity through integrated biochemical degradation and physical processes. Comparative analysis revealed that the K values for COD, NH₃-N, TN, and TP in the Luan River exceeded those of the Yixun River by 0.02, 0.01, 0.01, and 0.01 day⁻¹, respectively. The lower K observed in the Yixun River signified diminished pollutant removal efficiency, directly degrading the RAC. This correlation further indicated the regulatory role of river network hierarchy (e.g., Strahler stream order) in shaping RAC dynamics, where higher-order systems (e.g., the Luan River) exhibited enhanced self-purification potential compared to lower-order

Table 3
Setting of regulatory levels and scenarios for the four WQPs from domestic point source (DPS), industrial point source (IPS), non-point source (NPS) pollution, and ecological water supply (WS).

Regulatory scenario	Regulatory level	Reduction rate of DPS				Reduction rate of IPS				Reduction rate of NPS				Increase rate of WS			
		COD	NH ₃ -N	TN	TP	COD	NH ₃ -N	TN	TP	COD	NH ₃ -N	TN	TP	COD	NH ₃ -N	TN	TP
Baseline	0	0 %	0 %	0 %	0 %	0 %	0 %	0 %	0 %	0 %	0 %	0 %	0 %	0 %	0 %	0 %	0 %
Low	1	24.526 %	16.929 %	10.446 %	13.665 %	20.207 %	16.421 %	11.021 %	11.510 %	10 %	10 %	10 %	2 %	2 %	2 %	2 %	2 %
Moderate	2	34.762 %	23.143 %	15.659 %	18.793 %	27.735 %	22.586 %	14.842 %	16.269 %	20 %	20 %	20 %	4 %	4 %	4 %	4 %	4 %
High	3	44.996 %	29.357 %	23.921 %	20.872 %	35.263 %	28.751 %	18.663 %	21.028 %	30 %	30 %	30 %	6 %	6 %	6 %	6 %	6 %

Table 4
Key parameters of the MIKE 11 model for RAC calculations.

Simulated river	Diffusion coefficient (m ² /s)	Manning roughness coefficient	Attenuation coefficient (1/d)			
			COD	NH ₃ -N	TN	TP
Luan River	14–19	0.022–0.054	0.18	0.12	0.14	0.12
Yixun River	12–16	0.024–0.061	0.16	0.11	0.13	0.11

tributaries. The reliability of K estimates was supported by minimal RE in model calibration and validation. Specifically, the average RE values during the calibration and verification periods were 0.063 and 0.076 at the Litai station, and 0.077 and 0.060 at the Wulongji station (Fig. S2 and Table S1), respectively. A narrow discrepancy ($RE < 0.1$) was observed between the simulated and measured values of COD, NH₃-N, TN and TP at both stations, indicating that the model performed within acceptable accuracy standards (DHI, 2005).

Beyond the K parameter, stringent water quality standards may paradoxically induce negative RAC values, signifying a lack of residual assimilative capacity. Furthermore, overly conservative water quality thresholds (e.g., TP ≤ 0.1 mg/L in R₆) may artificially constrain RAC utilization and socioeconomic development (Tang et al., 2021; Chen et al., 2023). While physicochemical and regulatory factors dominated RAC dynamics, hydrological conditions—specifically flow discharge and velocity—also emerged as critical parameters (Wang et al., 2019; Bui and Pham, 2023). Spatially heterogeneous drivers, including land-use patterns, topography, and microclimate across different calculation units, significantly altered flow regimes, thereby directly modulating RAC. For example, during dry seasons in the Luan River Basin, drought-induced flow reductions diminished D and K . These hydrological constraints disrupted pollutant transport dynamics and biogeochemical transformation efficiency, thereby accelerating RAC depletion and potentially generating non-positive values (Zhao et al., 2018). Overall, these factors—hydrological constraints, biogeochemical limitations, and regulatory interventions—were incorporated into RAC calculations for subsequent watershed RAC assessments.

3.2.2. RAC assessment under the baseline

Understanding the RAC under the baseline scenario is a prerequisite for appropriately allocating AWC. Fig. 4 shows the results of RAC for the four WQPs in each calculation unit under the baseline. The RAC values for COD, NH₃-N, TN and TP revealed notable variations across the river basin. The lowest RAC values were observed for TN, ranging from -330.69 to -2896.60 kg/d across all calculation units, indicating a severe TN pollution load. More than half of the study area (R₂–R₆) exhibited negative RAC_{TP} values, suggesting insufficient remaining capacity to accommodate the TP load. Not strangely, intensive agricultural activities, such as excessive fertilizer use and livestock rearing, contributed to substantial nitrogen and phosphorus losses entering the river via runoff. Furthermore, the lower altitudes and reservoir retention effects in R₂–R₆ reduced the river sections' capacity to effectively dilute and assimilate pollutants. The discharge of TN and TP emerged as a primary source of non-point source pollution, posing a significant environmental concern due to the complexity of its discharge processes into the river (Chen et al., 2018). In contrast, positive RAC values for NH₃-N and COD were observed in all calculation units except R₃ and R₄. The absence of remaining assimilative capacity for COD in R₃ and R₄ (RAC_{COD} < 0) was attributed to their locations in urban centers and river confluences, where concentrated domestic and industrial activities led to significant point source pollution. R₃, with the highest GDP and population density among the eight calculation units, exemplified the influence of socioeconomic development on RAC (Li et al., 2023). Moreover, the river confluence in R₃ received pollutants from both the upstream main channel and tributaries with hydrodynamic interactions disrupting pollutant diffusion and attenuation; its geographical position is illustrated in Fig. 1d. These findings are consistent with Zhao et al.

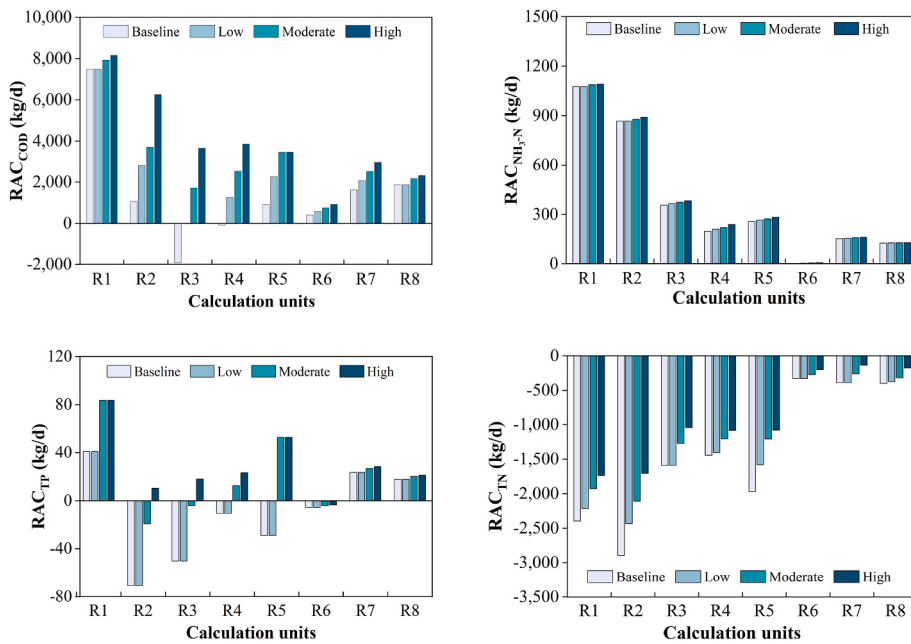


Fig. 4. River assimilative capacity (RAC) of the four water quality parameters (WQPs) in each calculation unit under different regulatory scenarios.

(2018), who emphasized the significant impact of pollutant attenuation rates on RAC.

The water quality objective played a crucial role in the RAC assessment. R₆ displayed relatively unfavorable RAC results, including the lowest RAC for NH₃-N, the third-lowest RAC for COD, and negative RAC values for TP and TN. Despite these concerns, statistical data indicated a relatively acceptable water quality in R₆. This was largely because R₆'s stricter water quality objective (Class II) served as a conservative benchmark. It functioned as a critical drinking water source protection zone near the Miaogong Reservoir in the upper reach of the Yixun River (Hebei Province Water Resources Document [2017] No. 127). The

conservative RAC assessment emphasized the importance of setting rigorous water quality standards as precautionary measures to protect aquatic environments, particularly in areas essential to water security and human health.

Point and non-point source pollution exhibited distinct pollutant characteristics and discharge pathways, resulting in varying impacts on the RAC due to differences in physicochemical properties and biochemical reactions across calculation units (Kang et al., 2020). As shown in Figs. 4 and 5, higher pollutant loads of TN and TP from non-point sources were primarily concentrated in the mainstream (R₁-R₅), with mean RAC values for TN and TP being 9179.55 and

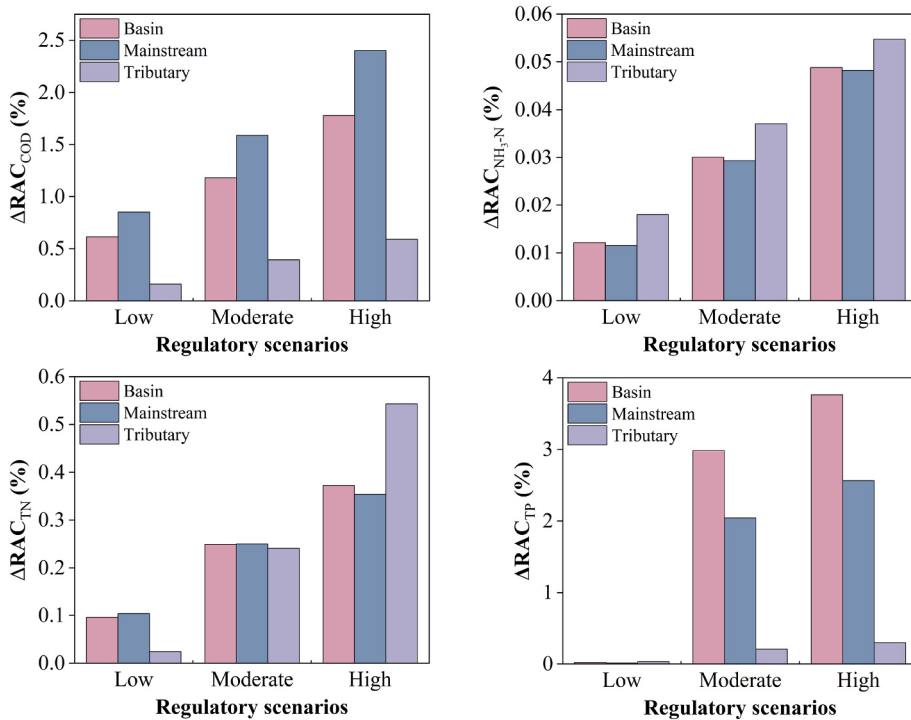


Fig. 5. Rate of change (%) in RAC (Δ RAC) for the four WQPs across river networks (basin, mainstream, tributary) under different regulatory scenarios.

155.49 kg/d lower in the tributary (R_6-R_8), respectively. Conversely, the Luan River exhibited higher RAC values for COD and $\text{NH}_3\text{-N}$, with values of 3558.34 and 2471.57 kg/d, respectively, greater than those of the Yixun River. This suggested that non-point source pollution was more severe in the mainstream, while point source pollution was more prominent in the tributary. These differences were attributed to variations in runoff intensity and frequency, land-use patterns, industrial structures, and hydrological and hydrodynamic conditions between the mainstream and tributary. R_1 exhibited the highest values of RAC for COD, $\text{NH}_3\text{-N}$, and TP, mainly due to its location at the uppermost reach of the Luan River. Aside from R_1 , positive RAC values for TP values were observed only in R_7 and R_8 in the Yixun River tributary, where regulation of the Miaogong Reservoir also significantly influenced the RAC. Overall, RAC varied among the eight calculation units mainly due to regional water quality objectives, basin characteristics, pollutant types, sewage discharge methods, and anthropogenic activities (Wang et al., 2021). Differences in subbasin characteristics at each calculation unit had significant impacts on RAC dynamics, particularly topography, hydrological-hydrodynamic processes, socio-economic activities, and water management goals.

3.2.3. Comparison of RAC under three regulatory scenarios

The RACs for the four WQPs in each calculation unit under the three regulatory scenarios were compared in Fig. 4. The comparison of RAC variations provides valuable insights into the effectiveness of each regulatory scenario in reducing specific pollutants. R_1 exhibited the highest increases in RACs for COD, $\text{NH}_3\text{-N}$, TN, and TP under moderate regulation, with increments of 432.18, 10.80, 292.35, and 42.76 kg/d compared to low regulation, respectively. This suggests that moderate

regulation provided the most significant improvements in pollutant reduction across all WQPs in R_1 . In R_2 , the RAC_{COD} showed the largest increase under high regulation, with an increase of 2554.38 kg/d. However, the RACs for $\text{NH}_3\text{-N}$ and TP showed the highest increases under moderate regulation, with values of 11.98 and 51.84 kg/d, respectively. In R_3 , the RACs for $\text{NH}_3\text{-N}$, TN, and TP exhibited the greatest increases under moderate regulation, with incremental values of 9.13, 318.42, and 46.13 kg/d, respectively. The most significant increase in the RAC_{COD} (1944.73 kg/d) occurred under high regulation, indicating the efficiency of targeting COD. Moreover, the RAC_{TN} exhibited the most significant increase in R_5 under moderate regulation, with an increase rate of 63.00 %, largely due to reductions in DPS and NPS based on orthogonal experimental analysis (Table 5 and Table S7). Additionally, R_6 showed significant increases in RAC for $\text{NH}_3\text{-N}$, with increase rates of 43.97 %, 60.16 %, and 70.83 % under low, moderate, and high regulation when compared with baseline, respectively. R_7 was an effective regulatory area under high regulation, with significant reductions in DPS, NPS, and ecological WS (Table 5 and Table S9). The presence of the Miaogong Reservoir and other water conservancy projects in the upper reaches of the Yixun River in R_7 suggested an obvious dilution effect on TN. The results highlighted the combined effect of pollutant reduction and water supply on RAC in different calculation units (Kang et al., 2020; Li et al., 2023).

The RACs in the mainstream and tributary rivers exhibited significantly different responses to regulation, as shown in Fig. 5. The RACs for COD and $\text{NH}_3\text{-N}$ in the Luan River (R_1-R_5) were 3558.24 and 2471.57 kg/d higher than those in the Yixun River (R_6-R_8), respectively, suggesting that the mainstream had a greater capacity to accommodate point-source pollution compared to the tributary. In contrast, the RACs

Table 5

Significance analysis of contributing factors on RAC of the four WQPs in each calculation unit (*P < 0.05, **P < 0.01).

WQP	Factors	R1	R2	R3	R4	R5	R6	R7	R8	WQP	R1	R2	R3	R4	R5	R6	R7	R8
COD	A1-DPS		**/	**/	**/					NH ₃ -N		**/	**/					
	A1-NPS	**/	**/								**/	**/						**/
	A2-DPS			**/	**/	**/							**/	**/	**/			
	A2-IPS			**/	**/	**/					**/			**/	**/			
	A2-NPS																	
	A3-DPS		**/															
	A3-NPS																	
	A4-DPS					**/	**/	**/										
	A4-IPS					**/												
	A4-NPS					**/												
TN	A5-DPS									TP								
	A5-IPS																	
	A5-NPS																	
	WS																	
	A1-DPS		**/	**/														
	A1-NPS	**/	**/	**/	**/	**/					**/	**/	**/	**/	**/			
	A2-DPS			**/	**/	**/												
	A2-IPS			**/														
	A2-NPS			**/														
	A3-DPS		**/															
NPS	A3-NPS			**/														
	A4-DPS						**/	**/	**/									
	A4-IPS						**/											
	A4-NPS																	
	A5-DPS																	
	A5-IPS																	
WS	A5-NPS																	
	WS																	

for TN and TP in the Luan River were 9179.55 and 155.50 kg/d lower than those in the Yixun River, respectively, indicating that the mainstream experienced more severe non-point source pollution. In the tributary, the regulation of COD had the most significant responses among the WQPs, with RAC increases of 16.00 %, 39.34 %, and 59.03 % under low, moderate, and high scenarios, respectively. In the mainstream, the reduction in TP was significant under moderate and high regulation, with RAC increases of 204.35 % and 256.31 %, respectively.

The RACs of the four WQPs improved with increasing regulatory levels, whereas the magnitude of these increments varied across scenarios (Fig. 6a). Under low regulation, the highest increase was observed for RAC_{COD} , with an increase rate of 61.43 %, followed by RAC_{TN} at 9.59 %. Comparatively, under moderate regulation, RAC_{TP} exhibited the largest increase at 298.43 %, followed by RAC_{COD} at 117.87 %. Under high regulation, RAC_{TP} also showed an obvious increase of 375.98 %, followed by RAC_{COD} at 177.95 %. When comparing different regulatory scenarios, the increase rates of RACs for COD and NH_3-N rose by 56.44 % and 1.79 % from low to moderate regulation, respectively, but they experienced smaller increases (3.64 % and 0.09 %) from moderate to high regulation. In contrast, the increase rates of RACs for TN and TP rose by 34.50 % and 298.43 % from low to moderate regulation, and by 22.15 % and 220.88 % from moderate to high regulation, respectively. Notably, the RAC for TP peaked under moderate regulation. These findings indicated that TN and TP from non-point source pollution could be effectively reduced even under lower regulation, while COD and NH_3-N from point source pollution needed relatively higher control. The results indicated that comparing the RACs of WQPs offered valuable information for developing targeted regulatory strategies, particularly by prioritizing key pollutant indices. Under all three regulatory scenarios, RAC_{TP} in R_2 and R_3 exhibited more significant increases than in other calculation units, indicating that reducing DPS and IPS should be prioritized in these regions. Conversely, RAC_{NH_3-N} was less sensitive to regulation, mainly due to its initially low concentration in the area. These results highlighted that regulatory effects varied significantly across different river sections even under the same regulatory level, especially between the mainstream and tributary. Consequently, implementing targeted regulation in specific river sections with key pollutant indices offered an effective approach to addressing localized pollution challenges and optimizing RAC allocation.

3.3. Optimal allocation of RAC under different regulatory scenarios

3.3.1. Selection of evaluation indices for the modified EGC

Achieving absolute fairness in RAC allocation was impossible, since the influencing mechanism of dynamic RAC was not confined to a single aspect (Zhao et al., 2018). Therefore, a multi-criteria evaluation system was used to calculate the modified EGC. The differences in natural environmental characteristics and socioeconomic development across

the eight calculation units were comprehensively considered, and redundant indices with overlapping information were excluded. Overall, the selection of evaluation indices was flexible, allowing adaptation to different stakeholders and practical applications in other river basins (Liang et al., 2015; Kang et al., 2020). The evaluation indices were selected to reflect economic, social, environmental, and ecological concerns (Sun et al., 2013b; Guo et al., 2021). Socioeconomic data from the Chengde Statistical Yearbook (2018) were employed to measure the influence of human disturbances on water pollutant discharges. Detailed information for each calculation unit is provided in Table 1.

Numerous studies have suggested that regions with higher population densities should implement greater reductions in pollutant discharges (Du et al., 2006; Wu et al., 2019). The study area has experienced rapid population growth, with an urbanization rate of 52 %, further exacerbating the imbalance between water supply and demand. Therefore, population was selected as a key evaluation index. GDP, a widely recognized indicator of economic development, was also included; higher GDP levels are associated with increased water consumption and pollutant discharges (Sun et al., 2010; Li et al., 2023). Therefore, regions contributing more significantly to GDP had a responsibility to reduce pollutant discharges (Xu et al., 2024). Moreover, the unsustainable and intensive use of land resources aggravated the relationship between aquatic ecosystems and socio-economic development. Larger land areas are typically correlated with higher potential pollutant discharges, as non-point source pollution is closely linked to surface runoff (Chen et al., 2018; Ji et al., 2022). Accordingly, the modified EGC model was constructed with three evaluation indices (i.e., population, GDP, and land area) as the abscissa, and with RAC as the ordinate.

3.3.2. RAC allocations via the modified optimization model

The modified EGC linked RAC and evaluation indices under different regulatory scenarios, providing valuable insights for developing fairness-based allocation schemes in specific regions (Feng et al., 2021). The minimal modified EGC indicated an ideal allocation based on fairness, as shown in Fig. 6b. In this study, an optimization model was proposed with an objective function of minimizing the ratio of modified EGC variation to environmental benefit variation (Fig. 6c). In the status quo, the G values for NH_3-N and TN were relatively lower (<0.7), whereas G values for COD and TP were higher (<2) (Fig. 6b). This indicated that the study area encountered significant challenges in achieving fairness-based RAC allocation for key pollutant indices, particularly COD and TP. Among the scenarios, the largest EGC occurred at the status quo, highlighting the need for regulation to optimize RAC allocation. Under the low regulatory scenario, only RAC_{NH_3-N} realized positive values in all calculation units, ranging from 3.43 kg/d (R_6) to 1076.37 kg/d (R_1), whereas RAC_{COD} , RAC_{TN} , and RAC_{TP} achieved some negative values (Fig. 6a). The G values for COD, NH_3-N , and TN decreased significantly relative to the baseline, indicating an effective

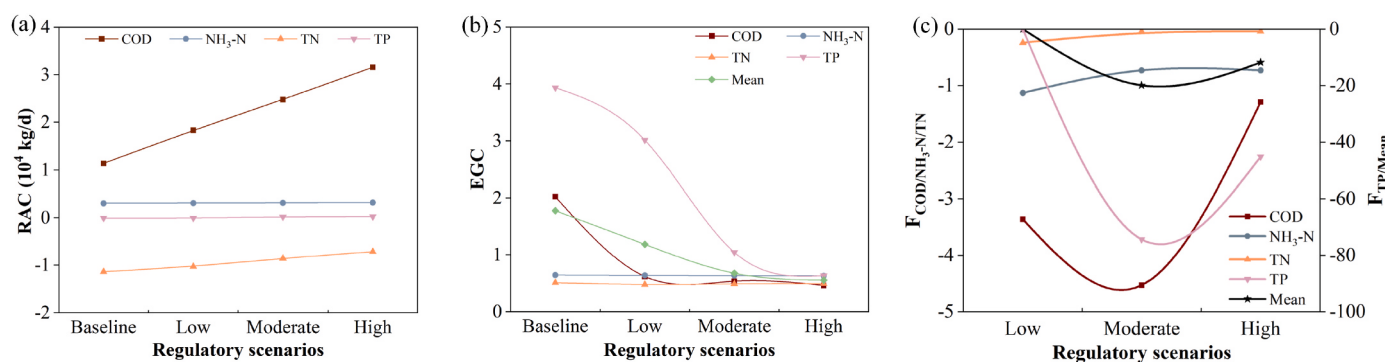


Fig. 6. Comparison of (a) RAC values (10^4 kg/d), (b) the modified EGC, and (c) objective function values (-10^5) for the four WQPs under different regulatory scenarios.

improvement in fairness-based RAC allocation (Fig. 6b). The largest reduction in G was observed for COD, with a decrease rate of 69.54 %, indicating that COD responded well to fairness-based regulation. Correspondingly, the largest RAC was observed for COD, with the highest increase rate of 83.45 % (Fig. 6). However, the G for TP exhibited little variation, with a decrease rate of 23.44 %, suggesting limited regulatory effects for TP under low regulation. Under the moderate regulatory scenarios, all G values for the four WQPs decreased by 73.59 %, 1.25 %, 4.14 %, and 73.49 % compared to the baseline, respectively. Compared with the low regulation scenario, the G for COD, NH₃-N, and TP continued to decrease, especially for TP with a significant decrease rate of 65.37 %; while the G for TN slightly increased by 2.10 %. Furthermore, positive RAC values were recorded for COD ($>751.68 \text{ kg/d}$) and NH₃-N ($>4.82 \text{ kg/d}$) in all calculation units. Under the high regulatory scenarios, the average G values were 1.22, 0.63, and 0.12 lower than those under the initial state, low, and moderate regulation, respectively. When compared with the moderate regulation, the G values for COD, NH₃-N, and TP decreased by 14.04 %, 0.79 % and 39.69 %, respectively; and the G for TN was stable. The smallest modified G was observed under high regulation (0.55), followed by 0.67 under moderate regulation. These results indicated that the ideal allocation of RAC was under high regulation based on environmental fairness.

Notably, the objective function was minimized under moderate regulation, with a value 69 % lower than that under high regulation (Fig. 6c). This indicated that moderate regulation provided the optimal allocation for the region by balancing fairness and efficiency. Within this framework, the responses of TN and NH₃-N to regulation were significant, with the objective function showing a notable decrease under low regulation. The moderate regulation scenario demonstrated the most effective control over COD and TP. These findings highlighted the importance of identifying key pollutant indices using different regulatory levels. Aligned with the *Chengde City Master Plan* (2016–2030) (<https://www.chengde.gov.cn>), which designated the study area as an ecological conservation function zone for the Beijing-Tianjin-Hebei region (Tian et al., 2019), this research offers valuable support for decision-making in pollutant discharge control and allocation.

3.3.3. Adaptability of the RAC allocation framework

While our findings derive from the Luan River Basin case study, the framework provides an adaptable methodology for watersheds with divergent land use patterns, hydrological regimes, or regulatory priorities. For instance, urbanized basins may prioritize point-source pollution (e.g., COD-dominated emissions) control through setting higher regulatory levels, while agricultural systems might implement spatially differentiated regulatory levels for RAC allocation to address non-point source pollutants like nitrogen runoff. Additionally, our framework's scenario design can be adapted by adjusting regulatory thresholds to align with local environmental goals. A basin prioritizing economic efficiency, for instance, could recalibrate the optimization model's objective function by reweighting fairness-efficiency trade-offs to reflect regional priorities.

Although the newly proposed framework has not yet undergone multi-basin validation, its reliance on readily accessible and publicly available datasets, such as hydrological and socioeconomic datasets, enhances its adaptability to regulated river basins. This framework enables policymakers to allocate pollutant discharge permits at sub-basin and sectoral levels (e.g., agriculture vs. industry), explicitly quantifying the critical trade-off between fairness and environmental benefits. Moreover, it potentially provides a theoretical foundation for guiding market-driven design, such as tradable discharge permit systems (Zhang et al., 2018; Tang et al., 2021). Under such systems, lower RAC zones could financially compensate higher RAC zones subject to high regulations, since the latter may bear more environmental costs (Sado et al., 2010; Jiang and Hellegers, 2016). Furthermore, our probability-distribution-based EGC modification offers a universal method for evaluating fairness in resource allocation. Its application can

extend to other environmental domains (e.g., carbon emission quotas) by adjusting regional disparity factors without altering its core structure (Zhang et al., 2023). Importantly, the integrated framework—which synergizes hydrodynamic-water quality coupling models, modified EGC, tiered scenario-based regulation, and multi-objective optimization for RAC allocations—delivers a replicable methodology to quantify fairness-efficiency trade-offs.

4. Conclusions

The study proposed an integrated framework for the optimal allocation of RAC to support decision-making on pollutant discharge control based on fairness-efficiency trade-offs. This framework was applied to the case study of the Luan River Basin in Chengde City. Hydrodynamic and water quality modules, orthogonal experiments, and the modified EGC were integrated into a novel optimization model for RAC assessments and allocations under different regulatory scenarios. The objective function aimed at minimizing the ratio of the modified EGC variation to environmental benefit variation. The initial state represented the least favorable condition, with the lowest RAC (90.53 kg/d) and the highest EGC (1.78). All RAC_{TN} and more than 50 % of RAC_{TP} were negative values, suggesting relatively severe non-point source pollution. Under high regulation, the average modified EGC was significantly reduced by 68.97 %, 53.49 %, and 18.22 % compared to the initial, low, and moderate scenarios, respectively. While high regulation achieved the ideal allocation based on environmental fairness, the moderate regulatory scenario realized the optimal allocation with the minimal objective function, considering the fairness-efficiency trade-offs. TP and COD exhibited the highest efficiency under moderate regulation, while TN and NH₃-N responded rapidly to regulatory measures. The study demonstrated how pollutant types, hydrological and hydrodynamic conditions, and socio-economic activities influence RAC. This framework provides valuable insights for decision-makers and stakeholders to implement differentiated regulatory levels and prioritize key pollutant indices across various river sections. By achieving the optimal allocation of RAC, this framework promotes ecological sustainability and improves resource efficiency in water quality management.

CRediT authorship contribution statement

Zhimin Yang: Writing – original draft, Methodology, Formal analysis, Data curation, Conceptualization. **Jiangying Wang:** Data curation. **Xiaoxuan Li:** Methodology, Data curation. **Chunhui Li:** Writing – review & editing, Supervision, Resources, Methodology. **Zaohong Pu:** Methodology, Funding acquisition. **Jing Hu:** Writing – review & editing, Data curation. **Yujun Yi:** Writing – review & editing, Conceptualization. **Xuan Wang:** Writing – review & editing. **Qiang Liu:** Validation.

Software and data availability

- Name of model: Integrated River Assimilative Capacity (RAC) Allocation Model based on Fairness-Efficiency Tradeoffs
- Developers: Zhimin Yang and Xiaoxuan Li
- Contact: yangzm@mail.bnu.edu.cn and chunhuili@bnu.edu.cn
- Date first available: January 5, 2024
- Data availability: The data used in this study, including hydrodynamic parameters, pollutant monitoring data, and orthogonal experimental design results for the Luan River Basin, are available upon reasonable request.
- Name of software: MIKE 11 Hydrodynamic and Advection-Dispersion Modules
- Developers: DHI (Danish Hydraulic Institute)
- Contact: DHI Support Portal at <https://service.mikepoweredbydhi.com> or email support at mike@dhigroup.com

- Date First Available: MIKE 11 was first released in the late 1980s. Specific module release dates can be confirmed in the version release notes provided on the DHI website
- Documentation: Comprehensive user manuals and technical documentation for MIKE 11 modules are available at <https://www.mikepoweredbydhi.com>

Declaration of competing interest

The authors declare that they have no known competing financial interests or personal relationships that could have appeared to influence the work reported in this paper.

Acknowledgments

This work was supported by the Joint Funds of the National Natural Science Foundation of China (U2243236), the National Key Research and Development Program of China (2022YFC3202001), National Science Fund for Distinguished Young Scholars (52025092), Open Fund of State Key Laboratory of Remote Sensing Science and Beijing Engineering Research Center for Global Land Remote Sensing Products (OF202208), and Innovative Research Group of the National Natural Science Foundation of China (52221003).

Appendix A. Supplementary data

Supplementary data to this article can be found online at <https://doi.org/10.1016/j.envsoft.2025.106503>.

Data availability

I have shared the link to my data at GitHub: <https://github.com/769057845/Paper-resources.git>.

References

- Arora, S., Keshari, A.K., 2021. ANFIS-ARIMA modelling for scheming re-aeration of hydrologically altered rivers. *J. Hydrol.* 601, 126635.
- Box, G.E., Jenkins, G.M., Reinsel, G.C., Ljung, G.M., 2015. Time Series Analysis: Forecasting and Control. John Wiley & Sons.
- Bu, J., Li, C., Wang, X., Zhang, Y., Yang, Z., 2020. Assessment and prediction of the water ecological carrying capacity in Changzhou city, China. *J. Clean. Prod.* 277, 123988.
- Bi, J., Lin, Y., Dong, Q., Yuan, H., Zhou, M., 2021. Large-scale water quality prediction with integrated deep neural network. *Inf. Sci.* 571, 191–205.
- Bui, L.T., Pham, H.T.H., 2023. Linking hydrological, hydraulic and water quality models for river water environmental capacity assessment. *Sci. Total Environ.* 857, 159490.
- Chinese Academy for Environmental Planning (CAEP), 2003. Guidance for Determination of National Water Environmental Capacity, p. 1e77. Beijing.
- Chen, Q., Wang, Q., Li, Z., Li, R., 2014. Uncertainty analysis on the calculation of water environmental capacity by an innovative holistic method and its application to the Dongjiang River. *J. Environ. Sci.* 26 (9), 1783–1790.
- Chen, L., Dai, Y., Zhi, X., Xie, H., Shen, Z., 2018. Quantifying nonpoint source emissions and their water quality responses in a complex catchment: a case study of a typical urban-rural mixed catchment. *J. Hydrol.* 559, 110–121.
- Danish Hydraulic Institute (DHI), 2003. MIKE 11, MikeNAM, MikeGIS User Guide and Scientific Documentation. Danish Hydraulic Institute, Hørsholm, Denmark.
- DHI, 2005. MIKE 11, Modeling System for Rivers and Channels. Danish Hydraulic Institute, Denmark.
- Du, Y.J., Li, Z.Z., Li, W.L., 2006. Effect of different water supply regimes on growth and size hierarchy in spring wheat populations under mulched with clear plastic film. *Agric. Water Manag.* 79, 265–279.
- Dai, C., Qin, X.S., Chen, Y., Guo, H.C., 2018. Dealing with equality and benefit for water allocation in a lake watershed: a Gini-coefficient based stochastic optimization approach. *J. Hydrol.* 561, 322–334.
- Feng, L., Li, Q., Zhang, L., Wang, H., Wang, W., Han, J., Li, B., 2021. Exploring the effect of floodgates operation systems on water environmental capacity in a regulated river network of Wuxi, China. *J. Clean. Prod.* 299, 126743.
- Gini, C., 1936. On the Measure of Concentration with Special Reference to Income and Statistics, vol. 208. Colo. Coll. Publ., Gen. Ser. No., pp. 73–79.
- Guo, C., Cui, Y., Shi, Y., Luo, Y., Liu, F., Wan, D., Ma, Z., 2019. Improved test to determine design parameters for optimization of free surface flow constructed wetlands. *Bioresour. Technol.* 280, 199–212.
- Guo, J., Zhao, M., Wu, X., Shi, B., Gonzalez, E.D.S., 2021. Study on the distribution of PM emission rights in various provinces of China based on a new efficiency and equity two-objective DEA model. *Ecol. Econ.* 183, 106956.
- Haire, M., Vega, R., Koenig, J., Rafi, T., 2009. Handbook for developing watershed TMDLs. In: Agency, U.S.E.P. (Ed.), Office of Wetlands, Oceans and Watersheds. Washington D.C.
- Hu, Z., Chen, Y., Yao, L., Wei, C., Li, C., 2016. Optimal allocation of regional water resources: from a perspective of equity-efficiency tradeoff. *Resour. Conserv. Recycl.* 109, 102–113.
- Hyndman, R.J., Athanasopoulos, G., 2018. Forecasting: Principles and Practice. OTexts.
- He, C., Liu, Z., Wu, J., Pan, X., Fang, Z., Li, J., Bryan, B.A., 2021. Future global urban water scarcity and potential solutions. *Nat. Commun.* 12 (1), 1–11.
- Jiang, Y., Hellegers, P., 2016. Joint pollution control in the Lake Tai Basin and the stabilities of the cost allocation schemes. *J. Environ. Manage.* 184 (Pt 3), 504–516.
- Ji, H., Peng, D., Fan, C., Zhao, K., Gu, Y., Liang, Y., 2022. Assessing effects of non-point source pollution emission control schemes on Beijing's sub-center with a water environment model. *Urban Clim.* 43, 101148.
- Kang, A., Li, J., Lei, X., Ye, M., 2020. Optimal allocation of water resources considering water quality and the absorbing pollution capacity of water. *Water Resour.* 47 (2), 336–347.
- Lee, C.S., Wen, C.G., 1996. River assimilative capacity analysis via fuzzy linear programming. *Fuzzy Set Syst.* 79 (2), 191–201.
- Liang, S., Jia, H., Yang, C., Melching, C., Yuan, Y., 2015. A pollutant load hierarchical allocation method integrated in an environmental capacity management system for Zhushan Bay, Taihu Lake. *Sci. Total Environ.* 533, 223–237.
- Liu, J.Y., You, X.G., Shi, X., Bao, K., Meng, B., 2016. Hydrological and ecological effects of dams in Luanhe River Basin. *Water Resour. Prot.* 32 (1), 23–28+35 (in Chinese).
- Lamontagne, J.R., Barber, C.A., Vogel, R.M., 2020. Improved estimators of model performance efficiency for skewed hydrologic data. *Water Resour. Res.* 56 (9), e2020WR027101.
- Lafta, A.A., 2022. Numerical assessment of Karun river influence on salinity intrusion in the Shatt Al-Arab river estuary, northwest of Arabian Gulf. *Appl. Water Sci.* 12 (6), 124.
- Li, D., Zuo, Q., Zhang, Z., 2022. A new assessment method of sustainable water resources utilization considering fairness-efficiency-security: a case study of 31 provinces and cities in China. *Sustain. Cities Soc.* 81, 103839.
- Li, D., Zuo, Q., Jiang, L., Wu, Q., 2023. An integrated analysis framework for water resources sustainability considering fairness and decoupling based on the water resources ecological footprint model: a case study of Xinjiang, China. *J. Clean. Prod.* 383, 135466.
- Moriasi, D., Arnold, J., Van Liew, M., Binger, R., Harmel, R., Veith, T., 2007. Model evaluation guidelines for systematic quantification of accuracy in watershed simulations. *Trans. ASABE (Am. Soc. Agric. Biol. Eng.)* 50 (3), 885–900.
- Ministry of Ecology and Environment (MEE), 2016. Announcement on Issuing Information List of Water Quality Control Units during the "13th Five-Year" Period. Ministry of Ecology and Environment, Beijing.
- Qin, D., Wei, A., Lu, S., Luo, Y., Liao, Y., Yi, M., et al., 2013. Total water pollutant load allocation in Dongting lake area based on the environmental Gini coefficient method. *Res. Environ. Sci.* 26, 8–15.
- Rai, S., Jain, S., Rallapalli, S., Magner, J., Singh, A.P., Goonetilleke, A., 2024. Effect of varying hydrologic regime on seasonal total maximum daily loads (TDML) in an agricultural watershed. *Water Res.* 249, 120998.
- Sun, T., Zhang, H., Wang, Y., Meng, X., Wang, C., 2010. The application of environmental Gini coefficient (EGC) in allocating wastewater discharge permit: the case study of watershed total mass control in Tianjin, China. *Resour. Conserv. Recycl.* 54, 601–608.
- Sun, Q., Zhang, C., Yu, X., Li, J., Zhang, Y., Gao, Y., 2013a. Best management practices of agricultural non-point source pollution in China: a review. *Chinese J. Ecol.* 32 (3), 772–778 (in Chinese).
- Sun, T., Zhang, H., Wang, Y., 2013b. The application of information entropy in basin level water waste permits allocation in China. *Resour. Conserv. Recycl.* 70, 50–54.
- Shu, H., Xiong, P., 2018. The Gini coefficient structure and its application for the evaluation of regional balance development in China. *J. Clean. Prod.* 199, 668–686.
- Taylor, S.D., He, Y., Hiscock, K.M., 2016. Modelling the impacts of agricultural management practices on river water quality in Eastern England. *J. Environ. Manage.* 180, 147–163.
- Tian, Y., Jiang, Y., Liu, Q., Dong, M., Xu, D., Liu, Y., Xu, X., 2019. Using a water quality index to assess the water quality of the upper and middle streams of the Luanhe River, northern China. *Sci. Total Environ.* 667, 142–151.
- Tang, M., Li, Z., Hu, F., Wu, B., Zhang, R., 2021. Market failure, tradable discharge permit, and pollution reduction: evidence from industrial firms in China. *Ecol. Econ.* 189, 107180.
- Talukdar, P., Kumar, B., Kulkarni, V.V., 2023. A review of water quality models and monitoring methods for capabilities of pollutant source identification, classification, and transport simulation. *Rev. Environ. Sci. Biotechnol.* 22 (3), 653–677.
- U.S. Environmental Protection Agency (USEPA), 1984. Technical Guidance Manual for Performing Wasteload Allocations, Book: VII: Permit Averaging Periods. United States Environmental Protection Agency, Office of Water, Washington DC.
- Wu, C.F.J., Hamada, M.S., 2009. Experiments: Planning, Analysis, and Optimization, second ed. Wiley.
- Wu, W., Gao, P., Xu, Q., Zheng, T., Zhang, J., Wang, J., et al., 2019. How to allocate discharge permits more fairly in China? A new perspective from watershed and regional allocation comparison on socio-natural equality. *Sci. Total Environ.* 684, 390–401.
- Wang, Q., Liu, R., Men, C., Guo, L., Miao, Y., 2019. Temporal-spatial analysis of water environmental capacity based on the couple of SWAT model and differential evolution algorithm. *J. Hydrol.* 569, 155–166.

- Wu, J., Luo, J., Du, X., Zhang, H., Qin, S., 2022. Optimizing water allocation in an inter-basin water diversion project with equity-efficiency tradeoff: a bi-level multiobjective programming model under uncertainty. *J. Clean. Prod.* 371, 133606.
- Wang, X., Li, R., Tian, Y., Liu, C., 2021. Watershed-scale water environmental capacity estimation assisted by machine learning. *J. Hydrol.* 597, 126310.
- Wang, H., Guan, Y., Hu, M., Hou, Z., Ping, Y., Zhang, Z., Zhang, Q., Shang, F., Lin, K., Feng, C., 2024. Enhancing pollution management in watersheds: a critical review of total maximum daily load (TMDL) implementation. *Environ. Res.*, 120394.
- Wang, Y., Wang, H., Sun, J., Qi, P., Zhang, W., Zhang, G., 2025. Spatially optimized allocation of water and land resources based on multi-dimensional coupling of water quantity, quality, efficiency, carbon, food, and ecology. *Agric. Water Manag.* 309, 109340.
- Xie, Y.L., Xia, D.H., Huang, G.H., Ji, L., 2018. Inexact stochastic optimization model for industrial water resources allocation under considering pollution charges and revenue-risk control. *J. Clean. Prod.* 203, 109–124.
- Xie, Q., Xu, Q., Rao, K., Dai, Q., 2022. Water pollutant discharge permit allocation based on DEA and non-cooperative game theory. *J. Environ. Manage.* 302 (Pt A), 113962.
- Yan, D.H., Wang, G., Wang, H., Qin, T.L., 2012. Assessing ecological land use and water demand of river systems: a case study in Luanhe River, North China. *Hydrol. Earth Syst. Sci.* 16 (8), 2469–2483.
- Yu, S., He, L., Lu, H., 2016. An environmental fairness based optimisation model for the decision-support of joint control over the water quantity and quality of a river basin. *J. Hydrol.* 535, 366–376.
- Yuan, Q., McIntyre, N., Wu, Y.P., Liu, Y.C., Liu, Y., 2017. Towards greater socio-economic equality in allocation of wastewater discharge permits in China based on the weighted Gini coefficient. *Resour. Conserv. Recycl.* 127, 196–205.
- Yue, Q., Zhang, Y., Li, C., Xue, M., Wang, T., 2021. Research of water environment capacity allocation in Liaoning province based on the analytic network process. *Water Resour.* 48 (2), 310–323.
- Zhao, C.S., Yang, S.T., Sun, Y., Zhang, H.T., Sun, C.L., Xu, T.R., et al., 2018. Estimating river accommodation capacity for organic pollutants in data-scarce areas. *J. Hydrol.* 564, 442–451.
- Zhang, M., Ni, J., Yao, L., 2018. Pigovian tax-based equilibrium strategy for waste-load allocation in river system. *J. Hydrol.* 563, 223–241.
- Zhang, J., Zhang, C., Shi, W., Fu, Y., 2019. Quantitative evaluation and optimized utilization of water resources-water environment carrying capacity based on nature-based solutions. *J. Hydrol.* 568, 96–107.
- Zhao, T., Shi, J., Lv, L., Xu, H., Chen, D., Cui, Q., et al., 2020. Soil moisture experiment in the Luan River supporting new satellite mission opportunities. *Remote Sens. Environ.* 240, 111680.
- Zhu, K., Chen, L., Chen, S., Sun, C., Wang, W., Shen, Z., 2022. New framework for managing the water environmental capacity integrating the watershed model and stochastic algorithm. *Sci. Total Environ.* 816, 151659.
- Zhang, H., Zhang, W., Lu, Y., Wang, Y., Shan, Y., Ping, L., et al., 2023. Worsening carbon inequality embodied in trade within China. *Environ. Sci. Technol.* 57, 863–873, 2023.